

**A STUDY ON KEY EVENTS DETECTION IN BASEBALL
HITTING USING INERTIAL MEASUREMENT UNITS**



by

**GARDIYE PUNCHIHEWAGE NIROSHAN SUSITH GARDIYE
PUNCHIHEWA**

A Dissertation submitted in partial fulfillment for the
degree of Doctor of Philosophy

Course of Production Engineering

Department of Materials and Informatics

Interdisciplinary Graduate School of Agriculture and Engineering

UNIVERSITY OF MIYAZAKI

March 2022

Declaration of Authorship

I, Gardiye Punchihewage Niroshan Susuth Gardiye Punchihewa, declare that the dissertation titled, ‘A study on key events detection on baseball hitting using inertial measurement units’ has been composed solely by myself. I confirm that,

- This dissertation has not been submitted in whole or part, in any other degree granting institutions
- The work presented is original and my own, except where, state otherwise by reference and acknowledgement
- Any part of the work that has been done jointly by research group members are clearly mentioned in the respective articles published in academic journals

Date: March 2022

Signed: Gardiye Punchihewage Niroshan Susith Gardiye Punchihewa

Advisor: Associate Professor Go Yamako

Abstract

Title: A study on key events detection in baseball hitting using inertial measurement units

By Gardiye Punchihewage Niroshan Susith Gardiye Punchihewa

Efficient training methods are essential in any sport. Evidence-based scientific approaches are now being used to improve athletic performance and to reduce injuries. In baseball, pitching and hitting are considered primary activities, from which more attention has been given to pitching in examining the increase rate of injuries. A baseball thrown by a pitcher will reach to the batter less than half of a second to which batter needs to react accordingly. Therefore, baseball hitting is considered the single most difficult motion in any sport. Baseball hitting involves whole-body, moving in a very short period and thus require high speed motion measurement techniques to accurately analyze the motion. Hitting motion is a sequence of movements from lower-body to upper-body. Sports scientists have divided hitting motion into four phases (stance, wind-up, swing, and follow-through) for comprehensive hitting analysis. These phases are identified by key events including foot-off, foot-on and bat-ball impact. Optical motion capture system (OMCS) is a camera-based motion analysis system, widely used to analyze sport-specific movements. The key events are typically detected by cameras and force plates. OMCS however requires a fixed indoor

laboratory, which limits baseball hitting analyses under restricted settings, which is far from real baseball hitting. This dissertation describes a systematic approach using inertial measurement units (IMUs), a wireless sensor-based system to accurately detect key events to analyze baseball hitting in a real game environment.

The dissertation is organized as follows. Chapter 1 of the dissertation introduces baseball game and the importance of analyzing baseball hitting. OMCS has been used in hitting analyses with high accuracy. However, it is difficult to setup the system in real game conditions and thus limited to laboratory settings. Previous studies have not investigated baseball hitting in a real game condition. Aim of this study, therefore, to introduce a new feasible solution with high accuracy to evaluate hitting motion in a real baseball field.

Chapter 2 describes previous research in baseball hitting and motion analysis systems. Previous research has shown that, batter generates power from lower extremities and transfer the energy to upper body using trunk segments. Trunk motion therefore is crucial in timing and energy transferring to hit a baseball. Most of the OMCS laboratories have confined space. Hence, hitting movements have been evaluated by hitting a stationary baseball kept on a tee-pole (a vertical rubber pole). Thus, alternative motion analysis system is required to accurately monitor hitting motion in outdoor conditions. The IMU is a

miniaturized sensor unit consists of an accelerometer, a gyroscope, and a magnetometer.

IMUs can be attached on players' body segments to measure segmental orientation in 3D space. Joint angles can then be calculated by using the orientation data of the adjacent segments. Nevertheless, techniques have not been developed to detect important hitting events using IMUs and IMUs have not been validated to be used in hitting analysis.

The key events during hitting motion are detected using IMUs (200 Hz sampling rate) attached on pelvis and hands and the methods are explained in Chapter 3. Local acceleration peaks of the IMU attached on pelvis segment were corresponded with the foot-off and foot-on events, those detected by force plates of the conventional OMCS. Local hand acceleration showed peak value not far off the bat-ball impact, detected by the cameras of the OMCS with root mean square error (RMSE) of 9 msec. The accuracy of the impact time is compromised due to low sampling rate and tee hitting condition.

The hitting kinematics evaluated using IMUs (1000 Hz sampling rate) is described in Chapter 4. Trunk (Spine joint, pelvis, and thorax segments) and hand kinematics data during hitting were compared with those of the OMCS. Results showed excellent accuracy for angles (RMSE < 5°) and angular/linear velocities (Mean absolute error < 10%).

Requirement of employing devices with higher sampling rates to closely monitor the coordination of body-segments is also emphasized.

Trunk and hand motion at bat-ball impact decides the outcome of the batted-ball. Thus, close detection of the impact time is important for hitting analysis. A new algorithm was introduced to detect bat-ball impact using local peaks of acceleration data from IMUs for pitched balls in chapter 5. A microphone with 10kHz was utilized to accurately evaluate the impact time. It was shown that impact time should be detected within 4 msec to measure valid kinematics and error less than 2 msec is required for excellent kinematic accuracy at bat-ball impact. The algorithm could detect impact time within 1msec in RMSE. This study also recommended 500 Hz or higher sampling rates for hitting analyses.

Chapter 6 concludes the dissertation and future works.

Acknowledgements

First and foremost, I'm humbled to be born as a human being and my gratitude is paid to our forefathers lived on mother-earth because of whom modern world is rich of knowledge that is accessible to everyone. I pledge to continue their footsteps and wisely use limited resources available to uplift the precious life given to mankind for many generations to be born.

I would like to express my immense gratitude to my academic advisor, **Associate professor Go Yamako**, for his invaluable advice and guidance throughout my academic life at University of Miyazaki.

My heartfelt gratitude is expressed to **Professor Etsuo Chosa**, for accepting me to University of Miyazaki and providing all the facilities necessary to complete research work during my master's and doctoral courses.

I highly appreciate the guidance and advice provided by **Professor Gang Deng** and **Associate Professor Yasuko Inaba**, my co-advisors.

I also appreciate the **thesis committee members** for their valuable advice.

It would be just a dream to achieve academic excellence without the support of my beloved mother **Yamuna Kalyani**, my late father **G. P. Amarapala** and my two brothers **Yasith** and **Kokila**. It was only possible to stay away from home and focus on my studies because of their unconditional love and support. Thank you!

Special thanks should be expressed to the **Ministry of Education, Culture, Sports, Science and Technology (MEXT)** for providing a full scholarship to pursue my higher studies in Japan.

A sincere appreciation to **University of Miyazaki, Japan** and **University of Moratuwa, Sri Lanka (UoM²)** including all the academic and non-academic staff for their support and guidance to continuously improve my academic and intellectual knowledge.

A special note of appreciation to **Mr. Goshiro Ushiroda** for introducing me to University of Miyazaki and supporting my daily life in Japan.

Finally, a big thanks to all the past and present laboratory members, my friends all around the world for supporting and encouraging me to achieve my goals.

List of Publications

The dissertation titled, ‘Efficacy of inertial measurement units to detect important events in analyzing kinematics of baseball hitting’ is a unity of several publications.

Journal Articles

1. Niroshan G. Punchihewa; Go Yamako; Yuu Fukao; Etsuo Chosa, Identification of key events in baseball hitting using inertial measurement units. *Journal of Biomechanics*. 2019, 87, 157–160
2. Niroshan G. Punchihewa; Shigeaki Miyazaki; Etsuo Chosa and Go Yamako, Efficacy of inertial measurement units in the evaluation of trunk and hand kinematics in baseball hitting. *Sensors* 2020, 20, 7331
3. Niroshan.G. Punchihewa; Hideki Arakawa; Etsuo Chosa and Go Yamako, A hand-worn inertial measurement unit for detection of bat-ball impact during baseball hitting. *Sensors* 2021, 21(9), 3002

Conference proceedings

1. プンチヘーワー ニローシャン ジー, 後藤 和貴, 帖佐 悦男, 山子 剛, 慣性センサを用いた野球の打撃解析：キネマティクスパラメータの評価, バイオフロンティア講演会講演論文集, 2019, 2019.30 巻, セッション ID 2C26, p. 2C26-, 公開日 2020/02/2

Contents

- Declaration of Authorship** i
- Abstract** ii
- Acknowledgements** vi
- List of Publications** vii
- Contents** viii
- List of Figures** xii
- List of Tables** xv
- Chapter 1** 1
 - 1. Introduction 1
 - 1.1. Background 1
 - 1.2. Statement of the problem 3
 - 1.3. Purpose and significance of the study 4
 - 1.4. Outline of the dissertation 6
- Chapter 2** 7
 - 2. Motion capture in baseball hitting 7
 - 2.1. Review of literature 7
 - 2.2. Commercially available motion capture systems 13
 - 2.2.1. Optical motion capture system (OMCS) 14
 - 2.2.2. Markerless motion capture system 16
 - 2.2.3. Electromagnetic tracking system 17

2.2.4.	Inertial measurement system	18
2.3.	Hitting analysis in baseball game environment	27
2.4.	Research implementation	29
Chapter 3	31
3.	Detection of the important hitting events using inertial measurement units	31
3.1.	Introduction	31
3.2.	Methodology.....	35
3.2.1.	Participants	35
3.2.2.	Hitting styles.....	35
3.2.3.	Instrumental setup.....	36
3.2.4.	Data processing.....	39
3.3.	Statistical analysis.....	42
3.4.	Results	42
3.4.1.	Foot-off and foot-on events	42
3.4.2.	Impact event	43
3.5.	Discussion.....	44
3.5.1.	Foot events.....	45
3.5.2.	Impact event	45
3.5.3.	Limitations.....	46
3.5.4.	Summary.....	46
Chapter 4	48

4. Efficacy of inertial measurement units in analyzing baseball hitting motion	48
4.1. Introduction	48
4.2. Methodology	49
4.2.1. Participants	49
4.2.2. Instrumental setup	50
4.2.3. Data collection.....	51
4.3. Statistical analysis	58
4.4. Results	59
4.4.1. Description of the baseball swing using IMUs	59
4.4.2. Validity and reliability of the IMUs.....	61
4.5. Discussion	64
4.5.1. Hitting characteristics.....	64
4.5.2. IMU measurement accuracy.....	65
4.5.3. Limitations	66
4.5.4. Summary	66
Chapter 5.....	67
5. Detection of the ball impact in pitched hitting condition using a hand worn inertial measurement unit	67
5.1. Introduction	67
5.2. Methodology	68
5.2.1. Participants	68

5.2.2.	Instrumental setup.....	69
5.2.3.	Data collection during in-field hitting	70
5.2.4.	Impact detection using microphone.....	71
5.2.5.	Impact detection algorithm.....	72
5.3.	Statistical analysis.....	77
5.4.	Results	79
5.4.1.	Deviation of the kinematics values from impact.....	79
5.4.2.	Impact time error	80
5.5.	Discussion.....	81
5.5.1.	Accuracy of bat–ball impact timing	82
5.5.2.	Hand acceleration caused by impact force	84
5.5.3.	Limitations.....	85
5.5.4.	Summary.....	86
Chapter 6	87
6.	Conclusion and future recommendations.....	87
6.1.	Conclusion.....	87
6.2.	Future recommendations	89
Appendix A	91
Appendix B	93
Appendix C	97
References	100

List of Figures

Figure 1: Optical motion capture system and reflective marker attachment.....	15
Figure 2: Inertial measurement units attached on hand segments	18
Figure 3: Flow diagram of the extended Kalman filter	23
Figure 4: Flow diagram of the nonlinear complementary filter	24
Figure 5: Flow diagram of the Madgwick filter	25
Figure 6: Phases of baseball hitting	32
Figure 7: Important events to be detected during hitting.....	34
Figure 8: Different hitting styles based on front foot movement	36
Figure 9: IMU attachment on body segments.....	37
Figure 10: Hitting trials off a tee pole. Global reference system is dented in XYZ...	38
Figure 11: Typical graphs of foot event comparison. Top graphs are pelvis acceleration towards Y direction and bottom graphs are the respective force plate data.....	40
Figure 12: Impact time detection using local acceleration of the hand IMU. vertical broken represents impact time detected by OMCS	41
Figure 13: Inertial measurement unit used in the current study. 500-yen coin was kept besides for size comparison	51
Figure 14: Trunk segments with respective local coordinates.....	54
Figure 15: Important events detected by IMUs (a) and hand velocity graphs from both systems.....	56

Figure 16: positioning of the inertial measurement units (IMUs) on body segments. (a) IMU attached on acrylic plate, (b) IMU on thorax, (c) IMU on pelvis, (d) IMU on hand	57
Figure 17: Pelvis angle and angular velocity calculated by inertial measurement unit (IMU) and optical motion capture system (OMCS). vertical lines in the graph represent the key events	60
Figure 18: Thorax angle and angular velocity calculated by inertial measurement unit (IMU) and optical motion capture system (OMCS). vertical lines in the graph represent the key events	60
Figure 19: Spine angle and angular velocity detected by inertial measurement units (IMUs) and optical motion capture system (OMCS). vertical lines in the graph represent the key events	61
Figure 20: Bland-Altman graph of the (a) Spine, (b) Thorax and (c) Pelvis angles at impact.....	63
Figure 21: Coordination of the key events and peak kinematic parameters of the trunk and hand segments	64
Figure 22: positioning of inertial measurement units (IMUs) on body segments	70
Figure 23: Hit map for pitched balls observed by visual inspection.....	71
Figure 24: microphone signal at bat-ball impact (a) before and (b) after signal rectification	72
Figure 25: Frequency spectrum of the hand acceleration (a) in free swing and (c) pitched hitting are on left. Corresponding resultant acceleration of the (b) free swing and (d) pitched hitting are on right.....	73
Figure 26: Hand acceleration data (a) before and (b) after using high pass filter.....	74
Figure 27: Filtered resultant acceleration profile. Impact time detected by the microphone is denoted with black dot	75

Figure 28: Filtered acceleration of the hand IMU (x, y, z local axes and corresponding resultant acceleration R) in different hitting outcomes. (a) Line drive, (b) Foul tip, (c) Ground ball, (d) Fly ball.....	75
Figure 29: Detection of local peaks in each axis of the hand acceleration and impact time detection	76
Figure 30: Impact algorithm flow chart.....	77
Figure 31: Overall hit count in different hitting outcomes	78
Figure 32: Kinematic profiles and corresponding deviation calculated as mean absolute error	80
Figure 33: (a) Impact error in aluminum and wooden bat in each tee and pitched bat session, (b) overall error distribution graph.....	83
Figure 34: Mean acceleration peaks in different outcomes after bat-ball impact.....	85
Figure 35: calibration box of the inertial measurement units	93
Figure 36: Regression graph of the measured and true values during accelerometer calibration	94
Figure 37: Data plotted in 3D space before and after magnetometer calibration.....	96

List of Tables

Table 1: Mean error and standard deviation (SD) root mean square error (RMSE), and intraclass correlation coefficient (ICC) of the pelvis peak position detected at the foot on event	43
Table 2: Mean error and standard deviation (SD), root mean square error (RMSE), and intraclass correlation coefficient (ICC) with 95% confident intervals (CI) at the events detected by inertial measurement units.....	44
Table 3: Root mean square error (RMSE) and mean absolute error (MAE) of the trunk segmental and spine angles	62
Table 4: Mean, bias and limit of agreement (LOA in upper and lower bounds (UB, LB)) and the corresponding intraclass correlation coefficient of the segmental and spine angles at impact and peak angular velocity	63
Table 5: Mean error, standard deviation and root mean square error of the impact time detected by new algorithm using hand acceleration	81
Table 6: Calibration data of the accelerometer	94

This dissertation is dedicated to

Sri Lanka baseball...

Chapter 1

1. Introduction

1.1. Background

Baseball is a team sport, popular in the American and East Asian sub-continent. Two teams compete against each other in which the team that scores most runs within 9 innings wins the game. Pitching and fielding are known as defensive plays to avoid scoring runs. Hitting and base running are called offensive plays to score runs against the defense. Even though the game continues for about 3 long hours, offense can usually score only 2 to 3 runs in professional baseball games. This is because the pitcher throws a baseball at about 145 kmh^{-1} velocity, 18.6 m away from the hitter. This will allow only about 400 msec for the hitter to predict the trajectory and the location of the ball to swing the bat to hit the pitched baseball. This is an extremely difficult thing to perform and thus, hitting a baseball is known as one of the most difficult sporting events [1].

Hitters try to hit the baseball as hard as they can to reach a base safely and bring the runners in to score. Speed and the trajectory of the batted ball are the deciding factors of a safe hit. A properly hit baseball with higher batted ball velocity and optimum trajectory may travel long enough to clear the fence, which is called a homerun, the highest achievement of a

single hit. Even with lower trajectories, hitters can reach the bases if the batted ball is fast enough to travel between infielders, or if the fielders make errors.

Hitter needs to maximize the bat end velocity to transfer momentum to the ball for higher batted-ball velocity. Energy is produced by the hitter from the lower body to upper body and the bat by utilizing the “kinetic chain”. Kinetic chain initiates with ground reaction forces. Then, linear and angular momentum is transferred from proximal to distal segments. An additional momentum is provided by the muscles of the proximal segments before transferring the momentum to the adjacent distal segment. Proper timing of energy production through muscles and subsequently transfer the momentum through segments will result maximizing the linear and angular velocity of the bat [2].

Timing of the momentum transferring is referred as the coordination of kinetic chain. Since pitchers try to change the speed and trajectory of the delivery to upset hitters’ timing, hitters should change their segment coordination accordingly to adjust for the incoming pitch. This is done by shifting weights from rear leg to the front leg at the early stage of the swing and timely rotate the trunk and hands to direct the sweet of the bat at the ball [3]. Many experienced hitters have different theories for an optimum bat swing. However, quantitative analysis is required to scientifically prove the statements given by the experts in the game to improve hitting performance.

Another aspect of analyzing hitting motion is to understand the underlying root cause of injury mechanism. More than 50% of abdominal muscle injuries in professional baseball are related to hitting [4]. An upward trend of abdominal muscle injuries has resulted loss of playing time and reinjury rate is as high as 12%. Hip and groin injuries are also common in baseball hitters [5]. Careful attention should be given to optimize hitting motion to reduce injuries. Study of baseball hitting will improve player performance and reduce injuries.

Early biomechanical analyses have explained the basic motion of the baseball swing [6-8]. Camera based motion capture systems have been utilized for baseball hitting analyses [9, 10]. Initial research available in the literature have used multiple video cameras using direct linear transformation [11, 12]. With the rapid development of hardware and software, high performance labs are now equipped with retro-reflective motion capture systems. High quality systems can capture marker trajectories at high sampling rates and currently, optical motion capture systems are considered “gold standard” for clinical studies[13-16]. Moreover, force platforms, strain gauges and electromyography (EMG) are being used to understand external forces on the body and muscle activities [17, 18].

1.2. Statement of the problem

Research related to kinematics and kinetics of baseball hitting has been performed using camera-based motion capture systems. Even though camera-based motion capture systems

are high in accuracy, main disadvantage of the camera system is it requires the cameras to setup in a confined space and thus difficult to establish in a real game environment such as in a baseball field. Therefore, hitting analyses have been performed inside laboratory settings. Most of the motion capture laboratories do not have enough space to hit for pitched baseball and thus involved hitting a stationary baseball. It has been shown that natural movement patterns differ when the participants were asked to perform gait movements inside laboratory settings [19]. An electroencephalography study has shown a significant difference in golf putting performance in laboratory and field conditions [20]. Environment conditions have a significant effect on human movement patterns. Therefore, hitting motion should be evaluated in real game scenario to effectively evaluate player performance.

1.3. Purpose and significance of the study

Improving player performance while reducing injuries will increase the spirit of the game for players, coaches as well as for fans. Motion analysis system is a useful tool to identify players' hitting attributes. However, optical motion capture systems, which use to analyze baseball hitting are very expensive and restricted inside laboratories. Moreover, players and coaches are required to visit research centers or universities to evaluate hitting motion. There is a high demand for a low-cost motion analysis system that can monitor hitting

movements during practice and game settings in a baseball field without high technical knowledge.

Therefore, the purpose of this study was to evaluate an alternative method to effectively analyze baseball hitting motion in a real game environment. Inertial measurement unit (IMU) is a wireless sensor unit. Several IMUs can be attached easily on player's body segments and kinematics such segmental orientation, angular velocity, and joint angles can be derived. However, kinematics measurements of the IMUs are not proved to be valid in analyzing hitting kinematics.

When analyzing baseball hitting, hitting motion is divided in to four phases (stance, wind-up, swing, follow-through) identified by foot-off, foot-on and bat-ball impact events. These events are typically detected using cameras and force plates, which are restricted to laboratory settings. IMUs are not able to use as a stand-alone system to analyze hitting motion due to lack of knowledge in detecting these important events. Therefore, main purpose of this study was to identify key events of baseball hitting using IMUs. Trunk and hand kinematics during baseball hitting was measured and compared it with OMCS.

The IMUs are low-cost system that can be easily used in both indoor and outdoor. Detection of the important events and validating the system for kinematic measurement will enable the sports scientists to evaluate hitting performance in real game conditions.

1.4. Outline of the dissertation

Chapter 2 describes motion analysis of baseball hitting, that have been depicted in previous literature. Advantages and disadvantages of the current motion analysis systems for hitting analyses are also explained. Key events that are necessary to describe hitting sequence are described in **Chapter 3**. Acceleration data of the IMUs attached on pelvis and hands were monitored and compared with conventional method to evaluate the accuracy of detecting key events. **Chapter 4** describes the calculation of trunk and hand kinematics using IMUs. Results were compared with gold standard motion capture system to evaluate the accuracy and reliability. Bat-ball impact is exclusively important in baseball hitting. Thus, variation of hitting kinematics when impact detection deviates from its exact value was compared for pitched balls in **Chapter 5**. A new algorithm to closely detect impact event was introduced using an IMU attached on hand. Finally, important points understood in this study are concluded in **Chapter 6** and future implementation of the methods introduced are discussed.

Chapter 2

2. Motion capture in baseball hitting

2.1. Review of literature

Baseball hitting motion was analyzed in early 60's using cinematographic evidence [8]. However, the first three-dimensional (3D) analysis of swinging a baseball bat was completed by Shapiro [10]. Direct linear transformation method was used with two video cameras to determine the 3D coordinates of the proximal and distal ends of the bat [11, 12]. Messier and Owens evaluated the bat dynamics of the female softball swing by using similar method [7]. They further used force plate data to analyze ground reaction forces to evaluate lower extremity kinetics along with the camera data to analyze hip and knee movements [9]. This is the first 3D biomechanical analysis carried out to evaluate bat swing.

Welch and others used a camera based motion capture system to describe the full-body mechanics of baseball hitting [21]. This study has aimed to understand the coordination and movement during baseball swing with the participation of professional baseball players. Six cameras were used to assess the movement of the body segments at 200Hz sampling rate. Force platforms were used to detect ground reaction forces at 1000Hz sampling rate.

There were two main findings of this analysis. They confirmed the concept of the “kinetic chain” when swinging a baseball bat. If explained briefly, kinetic chain is transferring momentum from larger base segment to smaller adjacent segments. In a system of multiple linked segments, significant amount of energy is consumed to move larger base segments to increase linear and rotational velocity which elevate the momentum. When the base segments decelerate, velocity of the adjacent smaller segments increases to conserve the total momentum of the system [22]. Each human body segment can generate power through the skeletal muscles. Thus, optimizing the momentum generated from the lower limbs to upper limbs through the kinetic chain will generate significant amount of power, which could not possibly be generated just by the upper limbs to hit a baseball over 100 m distance.

Second finding is to describe the hitting motion in sequence of phases. As it has been described for a right-handed hitter, swing motion starts with rotating the arms, shoulder, and hips clockwise while shifting the weight to the rear foot (Loading/stance phase). Then hitter pushes himself to the pitcher’s direction by applying force from rear foot to increase linear momentum (Wind-up/Stride phase). At the same time, arms and shoulders continue to rotate clockwise creating a coil-like effect in the trunk segment which separates lower and upper parts of the body. Once the front foot is planted on the ground to have a solid base support, hitter suddenly decelerates his linear momentum towards the pitcher which consequently transferring the momentum to rotate around the hips counterclockwise. This is the instant

where the linear momentum component interacts with the rotational momentum component.

As per the principle of kinetic chain, shoulders start rotating after the hips followed by the arms to create large momentum to increase bat velocity (Swing phase). Finally, after the bat-ball contact, hitter starts decelerating body segments using muscle forces to minimize the momentum to run towards the first base (Follow-through phase).

This paper has put up a solid foundation to describe biomechanics of baseball swing in professional athletes. However, this paper only described the motion by hitting a stationary baseball, which in fact limits the other psychological and physiological aspects of detecting the trajectory and speed of a moving baseball to physically prepare and react to hit.

Escamilla and others performed a hitting analysis to distinguish kinematic differences between youth and college level baseball players [23]. They have setup two synchronized video cameras in a baseball ground and manually digitized video data recorded at 120 Hz sampling rate. It has been shown that upper torso angle and angular velocity were significantly different between youth and adult hitters. Even though this study was performed to hit baseball thrown by a pitcher, low sampling rates and manual digitization using only 2 cameras compromises the accuracy and reproducibility of the results. Also, the sampling rate is too low to effectively measure baseball hitting mechanics.

Another study has been performed to evaluate kinematic differences of baseball swing with varying skills, using a sophisticated motion capture system with four cameras at 240Hz sampling rate [24]. Sub-elite baseball players were divided in to two groups based on their batting average and the ratings of experienced baseball coaches. Main difference between the two groups were identified as maximum hip angular velocity. High caliber hitters tend to have increased pelvis angular velocity than the low caliber players. This study also has performed inside laboratory condition and thus limited to hitting a stationary baseball off a tee pole.

A high-level study has been performed by Dowling and others to compare the kinematics of youth, high school, college, and professional baseball players [25]. They have used eight-camera motion capture system with 480 Hz sampling rate to capture hitting mechanics. Lead hip internal rotation has shown significantly different between the groups. Peak angular velocity of the pelvis and back elbow extension velocity have shown to be contributed to increased bat velocity. This analysis also has been performed under laboratory condition by hitting a stationary baseball and have stressed the importance of executing hitting analysis in natural game conditions to capture the best performance of hitting.

Baseball hitting is not only about hitting a baseball as hard as possible to travel long distance. Ability to carefully select the right pitch in the strike zone while coordination of body

segments to maximize the power are equally important to hitter's performance. A professional level baseball hitter requires about 200 msec to swing a bat [2, 6]. With incoming pitch at the range of 130 kmh⁻¹ to 145 kmh⁻¹, it will only get about 200 msec - 600 msec to determine the pitch location and trajectory. The decision-making process is generally explained by the perception-action coupling [26]. When the perceptual decision process is missing, the effect of the physiological action could be different. Lower limb kinetic comparison has been performed to differentiate the parameters of hitting during tee batting and pitched batting [27]. It has been shown that lower trunk angular velocity is greater in tee batting condition than pitched batting. Also, hitters take longer time to swing a pitched ball than hitting a stationary ball. this study has only measured lower limb parameters. It is fair to assume that kinematic and kinetic differences in the lower limbs can strongly influence the biomechanics of trunk and upper limbs when hitting a pitched ball compared to tee batting. Furthermore, kinematic difference between tee-batting and toss-batting training methods have been analyzed and shown that hitting movements are significantly different [28].

There are three main takeaways regarding the hitting analysis from previous literature.

1. Baseball hitting is a complex sequence of motion. Hitting a baseball requires the coordination of lower body and upper body. Trunk mechanics plays a major role in

transferring energy from lower to upper body and timing to hit a baseball.

2. Camera based motion capture systems have been used since 1960s to analyze baseball hitting. optical motion capture systems have been developed exponentially to capture high speed sports movements with high accuracy. However, setting up a camera system in a real baseball environment is difficult and thus hitting analyses are limited inside laboratory conditions. It is difficult to reproduce natural movements in real life inside a laboratory and thus biomechanical parameters differ when hitting analysis is performed inside a laboratory.
3. Since motion analysis laboratories have confined space, majority of baseball hitting analyses have been performed by hitting a stationary baseball off a tee pole. It is evident that biomechanical parameters are different between pitched and tee bat conditions.

There is a research gap in analyzing baseball hitting mechanics in game settings due to the limitations of camera-based motion capture systems. Alternative motion capture systems are available in the market. However, none of the systems have proven to be useful in analyzing baseball hitting mechanics due to lack of scientific evidence.

Purpose of this study was to investigate an alternative solution to accurately measure biomechanics of baseball hitting under natural game conditions. The new solution must consist of following conditions.

1. New method should not interfere any natural movements of hitting.
2. Should be able to use both indoor and outdoor conditions.
3. Reliability and accuracy to calculate biomechanics must be confirmed.
4. System calibration and set up time should be as minimum as possible so that data can be captured during match conditions.
5. Sampling rate should be higher than the current camera-based motion capture systems since previous research have addressed it as a limitation to accurately detect hitting motion.
6. Low cost and should be able to operate without high technical knowledge.

2.2. Commercially available motion capture systems

Human movement analysis is of an interest ever since. Quantification of human movement patterns were pioneered by Marey and Muybridge using photographic techniques [29, 30].

There was a need of an improved technique to understand human locomotion for the treatment of veteran soldiers of the World War II [16]. Development of cameras and video recording technologies together with the evolution of computer technology have provided advanced measuring techniques to quantify from gait analysis to highly dynamic sports movements.

In the context of human motion capture for sports applications, there are different technologies available to cater different purposes. Following section will briefly explain the motion capture systems and their advantages and disadvantages in various sports applications.

2.2.1. Optical motion capture system (OMCS)

Arguably the most accurate motion capture system available for human movement analysis is the optical motion capture system. OMCSs (e.g., VICON, OptoTrack, Qyalisys etc.) are regarded as the “Gold standard” in motion capture[13, 14, 31]. Modern OMCS uses spherical markers attached on the human body segments and three-dimensional (3D) position of each marker will be captured by multiple cameras fixed around capture volume (Figure 1). Markers can be active or passive. Active markers emit infrared (IR) light while passive markers are retro-reflective markers that reflect the IR light emitted from the cameras. Position of each camera will be calibrated using a Wand, with respect to an origin initiated during the calibration process. Marker trajectories are then measured respect to the origin in a 3D volume.

Accuracy of the trajectory measurement depends on several factors. Each marker should be captured by at least 2 or 3 cameras depending on the algorithm used by the respective software. Complex movement require many cameras to accurately detect marker trajectories.



Figure 1: Optical motion capture system and reflective marker attachment

Markers are attached on the skin. Skin artefacts are present when performing complex motions, which violates the rigid body assumption underlying the segmental orientation calculations. Also, markers can be occluded (interfering the line-of-sight) due to complex movements. Occluded markers create gaps in trajectory data. They can be filled with interpolation techniques, but the accuracy is compromised. Capture volume is determined during the initial calibration process. If the participant exists the calibrated volume, the accuracy of the marker trajectory will be decreased. At least 3 markers should be attached on a single segment to calculate 3D orientation. However, as mentioned before, markers can be occluded and therefore require multiple markers on a single body segment to increase

the accuracy of orientation estimation. Hardware limitations such as camera resolution and sample frequency are also affecting the accuracy of the measurement.

OMCS require fixed camera setup and thus the capture volume is fixed. Large number of cameras are required to increase the capture volume. This will increase the hardware cost, labor and moving the system outside the laboratory is cumbersome. Cameras detect the IR reflection in a specific frequency spectrum and bright sunlight may interfere the measurement [32]. Therefore, OMCS is usually setup inside a laboratory. When considering outdoor sports such as baseball, OMCS has practical disadvantages to be used in a real baseball field.

2.2.2. Markerless motion capture system

Markerless motion capture system (MMCS) uses single or multiple cameras to measure joint coordinates in 3-dimensional space. A depth sensor is usually incorporated when operating with a single camera. Advanced image analysis techniques, computer vision and machine learning algorithms have been used to develop software platforms to detect joint centers from moving images of human subjects. Focus of the development of MMCS is to reduce the preparation time in attaching markers on the body and make the system available outside laboratory settings. Since markers are not required, players are able to perform their motion, wearing sport-specific clothes. MMCS have proved good accuracy in sagittal plane

kinematic calculations of the slow movements but prone to higher error in rotational movements in the transverse plane [13]. Even though MMCS is a promising tool in the future of motion analysis in sports and rehabilitation, algorithms should be further optimized for highly dynamic sports [33].

2.2.3. Electromagnetic tracking system

Electromagnetic tracking (EMT) system operates solely on magnetic induction. A magnetic field generator creates a magnetic cloud in a specific volume. Position and orientation of a miniature sensor can be tracked by the system [34]. Wireless sensor modules are available. Therefore, a single sensor can be attached on a single body segment without movement restrictions. With multiple sensors attached on different body segment can track the position and segment orientation and joint angles can be calculated. Main advantage of the EMT over OMCS is that it does not require line-of-sight that would possibly lose tracking due to occlusion. EMT is mainly used in robotics and medical applications [35, 36]. Softball pitching analyses have been performed in controlled laboratory settings using EMT [37-39].

EMT can generate an adequate capture volume. However, the accuracy is less than that of OMCS. Main disadvantage of the EMT is magnetic field distortion due to the presence of ferromagnetic materials and the Eddy current in other electronic devices [40]. Also, the noise ratio increases as the distance between the sensor and the magnetic field generator

increases. Considering EMT to be used in a baseball field, magnetic field generator and the receiver need to be kept outside the field, which will increase the distance between receiver and the sensor that could reduce the accuracy. Baseball fields usually have back nets made of ferromagnetic materials which may affect when generating a magnetic field.

2.2.4. Inertial measurement system

Inertial measurement unit (IMU) is a sensor unit comprises with an accelerometer, gyroscope, or/and a magnetometer. Three sensors are compacted with a rechargeable battery inside a plastic package. Initially, IMUs were used in aircraft guidance control and underwater navigations [41].



Figure 2: Inertial measurement units attached on hand segments

Recently, IMUs are becoming popular in the motion analysis discipline [42-44].

Microelectromechanical systems (MEMS) technology is progressing exponentially with the

rapid development of smartphones and other mobile devices. Market capacity increased abruptly and low-cost, low-power IMUs are now available with high accuracy. Moreover, wireless technology is developing rapidly. This also helped the IMUs to be wireless with low power consumption. IMU can be easily attached on body segments and segmental orientation can be calculated to measure joint angles and other kinematics (Figure 2).

Accelerometer, gyroscope, and magnetometer will measure linear acceleration, angular rate and strength and the direction of the earth's magnetic north in three orthogonal axes respectively. However, each sensor has its own drawbacks and thus individual measurements cannot be used to calculate IMU orientation accurately.

2.2.4.7. *Sensor errors*

An ideal accelerometer will measure the linear acceleration in the direction of acceleration in three orthogonal axes. However, practical accelerometer records the instantaneous acceleration (\dot{v}) together with gravity (g), sensor bias (b_a) and noise (n_a). A practical model of an accelerometer is given in the below equation.

$$\mathbf{a} = \dot{v} + g + b_a + n_a \quad (2.1)$$

Gyroscope measure the angular velocity in three orthogonal axes. Gyroscope measurements are also contaminated with bias (b) and noise (n).

$$\boldsymbol{\omega} = \boldsymbol{\omega}_b + \mathbf{b} + \mathbf{n} \quad (2.2)$$

Unless the measurement environment is free of ferromagnetic materials and electronic devices that could possibly distort the magnetic flux, magnetometer measurements are usually subjected to distortion. These distortions can fall in to either hard iron or soft iron distortions. When the measurement volume consists of hardware that could create a magnetic field such as speakers or magnets, that will create a permanent hard iron distortion. Deflections or alterations of the existing magnetic field are known as soft iron distortions. Nickel or iron metals could affect such distortions.

Commercial IMUs have built-in orientation algorithms. However, accuracy and reliability of the proprietary algorithms are not proven for sports specific movements and unable to experiment with output result which may suffer from sensor drift and bias due to environmental conditions. However, there are open-source algorithms that have been developed to estimate IMU orientation. Some algorithms only use accelerometer and gyroscope data. Initial orientation of the IMU will be taken as the reference coordinate system to estimate the orientation over time. When multiple IMUs are used in the system, all the IMUs should be kept in the same direction before capturing the data to calculate orientation under common reference system. This is less practical for sports applications as calibration and preparation time should be minimal to collect data in game environment. To overcome this complication, some algorithms have included magnetometer data to estimate orientation with respect to a fixed reference system. Gravity vector from the accelerometer

and magnetic north derived from magnetometer are used as reference vectors to develop an earth fixed common reference system (North, East, Down: NED). These algorithms are commonly referred as attitude heading reference system (AHRS). In this research, only AHRS are considered because of its applicability in multi-sensor applications.

2.2.4.8. Open-source fusion algorithms

Angular velocity data taken from the gyroscope can be integrated with respect to time to calculate orientation from its previous position. However, the angular rates measured by the gyroscope drift over time, which result in accumulating error. To obtain better orientation estimation to compensate gyroscope drift, gyroscope data are fused together with acceleration and magnetic field data. There are many fusion algorithms available to estimate IMU orientation. Solution of these algorithms vary in terms of accuracy, stability and computational efficacy [45]. This section will only discuss the most-used fusion algorithms in literature related to motion analysis.

Mostly used techniques are extended Kalman filter, non-linear complimentary filter (Mahoney filter) and gradient-descent based fusion algorithm (Madgwick filter).

Extended Kalman filter

Kalman filter has been used widely to study the orientation estimation. The basic principle is that each measurement in real world data deviate small amount from the original value.

If the historic data were available, that could have been used to average out and estimate the next value. However, it requires lot of memory and computational time. Instead, Rudolf Kaman introduced to use the previous values to calculate a gain and predict current state [46]. This is explained in the state update equation.

$$\hat{X}_{n,n} = \hat{X}_{n,n-1} + K_n(Z_n - \hat{X}_{n,n-1}) \quad (2.3)$$

$\hat{X}_{n,n}$ = Estimated current state

$\hat{X}_{n,n-1}$ = Predicted value of the current state

K_n = Kalman gain

$(Z_n - \hat{X}_{n,n-1})$ = Residual value [Measurement – predicted current state]

The concept of the state update equation is used in orientation estimation algorithms.

Extended Kalman filter (EKF) is derived to linearize nonlinear systems with additive noise

[47]. Local linearization requires to compute the Jacobian of measurement state, dynamic

state, or both of the $\hat{X}_{n,n-1}$. The basic structure of the EKF is shown in figure 3 [47].

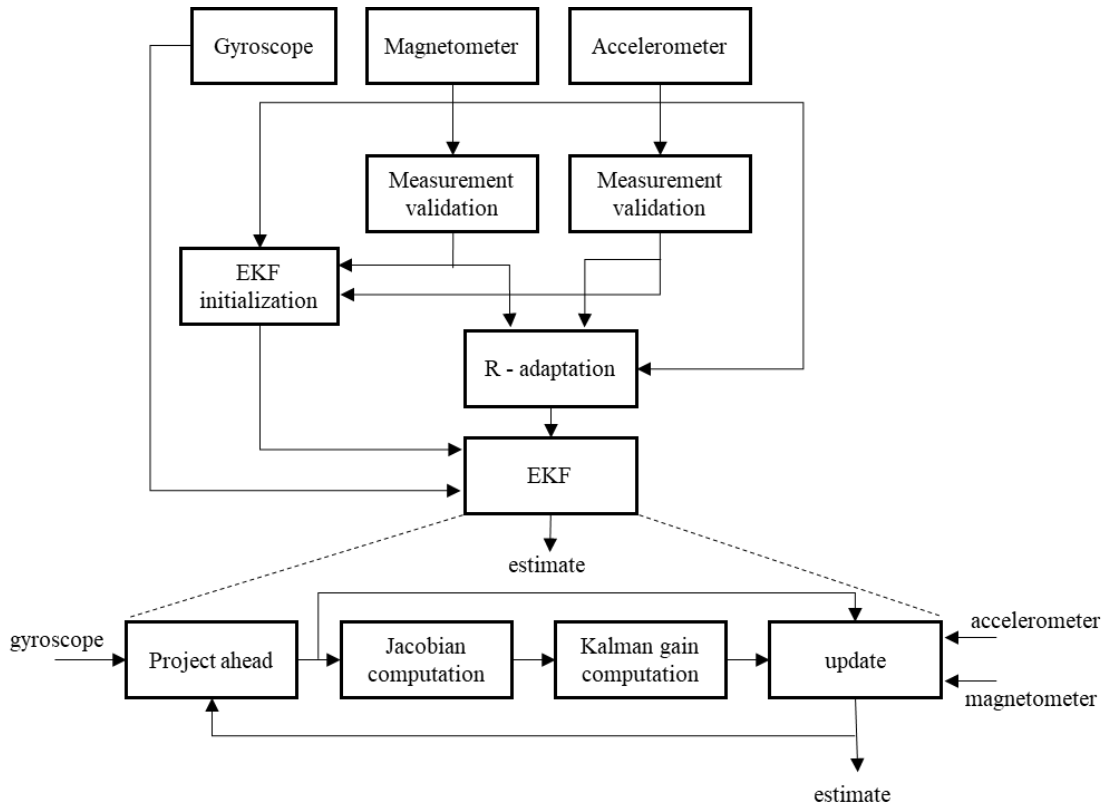


Figure 3: Flow diagram of the extended Kalman filter

EKF has been used for many years and different formulations has been introduced to increase accuracy of the orientation estimation. However, EKF models are complex and therefore difficult to fine-tune the parameters for proper implementation in different biomechanical applications [48]. Moreover, magnitude of the measurement variance is inversely proportional to the predicted estimation [49]. Therefore, IMU data required to be calibrated properly before using the EKF.

Non-linear complimentary filter

Complementary filters are developed to compensate the noise measurements in both low and high end of the frequency spectrum. Low cost IMUs have lower hardware resolution

yield to high noise levels. As gyroscope bias required to be constantly monitored, a linear solution is not desired when real time applications are concerned. Non-linear complementary filter provides the orientation as a deterministic observer on the special orthogonal group; $OS3$ [50]. This filter is generally referred as Mahony filter. Measured and estimated vectors of the gravity and the magnetic fields are cross multiplied, and the calculated error is used to correct the gyroscope bias (Figure 4).

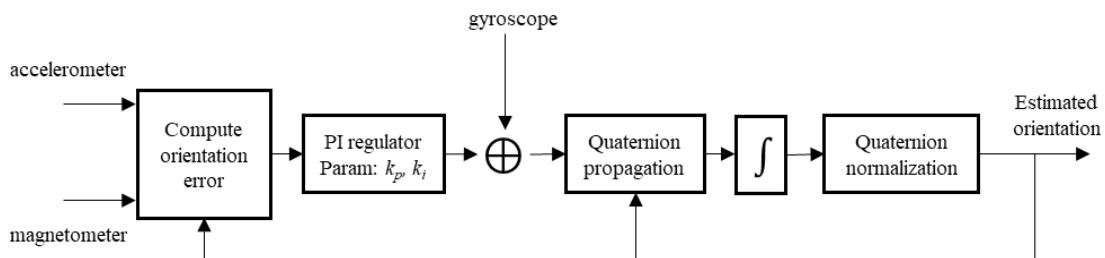


Figure 4: Flow diagram of the nonlinear complementary filter

A proportional integral (PI) regulator is used to correct the measured angular velocity. Rate of change of orientation is then formulated using the corrected angular velocity in the form of quaternion and the first integral is used to estimate the orientation of the current state. Two parameters of the PI regulator (K_p , K_i), known as filter gains should be calculated prior to data collection. The values for filter gains require trial and error method and authors have not mentioned a mathematical model to estimate the gains. Orientation estimation requires the value of the previous step and thus initial value need to be guessed. Therefore, the algorithm requires initial transient response time to reach steady state.

Gradient-descent fusion algorithm

As mentioned by name, this algorithm uses gradient-descent minimization problem to compensate gyroscope drift [51]. Commonly referred as Madgwick filter, this algorithm works in two phases (Figure 5).

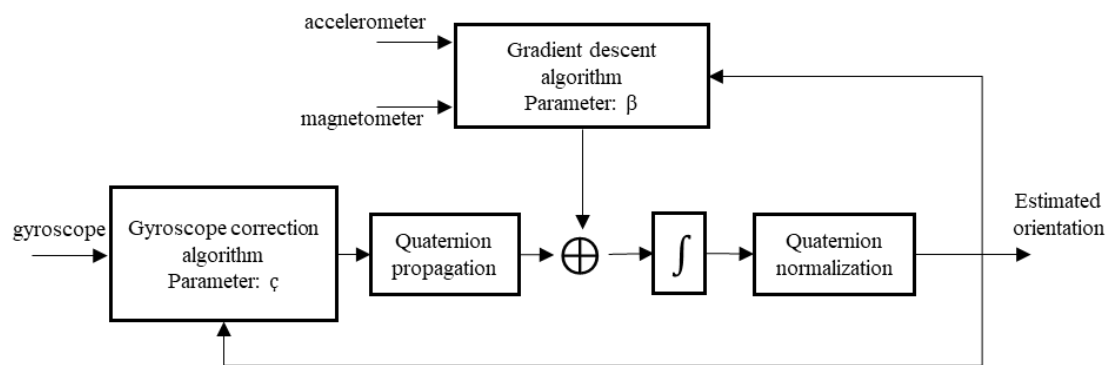


Figure 5: Flow diagram of the Madgwick filter

Initially, gyroscope measurements are aligned in a correction step. Bias and drift of the angular rates are used to compute the orientation of the IMU via quaternion propagation from the previous step, somewhat similar to Mahony filter. Madgwick filter uses an adjustable parameter β (filter gain) to fuse both acceleration and magnetic field vector using gradient-descent algorithm. Output of the fusion is then used to correct the estimated gyroscope measurement. Filter gain β can be calculated using the initial gyroscope bias [52].

Implementation of the Madgwick algorithm can be broken down into six steps.

Step 1: Normalize accelerometer $[a_x, a_y, a_z]$ and magnetometer data $[m_x, m_y, m_z]$

$$[\hat{a}_x, \hat{a}_y, \hat{a}_z] = [a_x, a_y, a_z] / \sqrt{a_x^2 + a_y^2 + a_z^2} \quad (2.4)$$

$$[\hat{m}_x, \hat{m}_y, \hat{m}_z] = [m_x, m_y, m_z] / \sqrt{m_x^2 + m_y^2 + m_z^2} \quad (2.5)$$

Step 2: Reference direction of the earth's magnetic field

$$h = q_{est,t-1} \otimes \hat{M}_t^s \otimes \hat{q}_{est,t-1}^* \quad (2.6)$$

$$b = [0, \sqrt{h(2)^2 + h(3)^2}, 0, h(4)] \quad (2.7)$$

where $\hat{M}_t^s = [0, \hat{m}_x, \hat{m}_y, \hat{m}_z]$, q is estimated quaternion and q^* is quaternion conjugate.

Step 3: Gradient-descent algorithm corrective step

$$F_{gb}(q_{est}, \hat{a}_s, \hat{b}_e, \hat{m}_e) = \begin{bmatrix} F_g(q_{est}, \hat{a}_s) \\ F_b(q_{est}, \hat{b}_e, \hat{m}_e) \end{bmatrix} \quad (2.8)$$

$$J_{gb}(q_{est}, \hat{b}_e) = \begin{bmatrix} J_g(q_{est}) \\ J_b(q_{est}, \hat{b}_e) \end{bmatrix} \quad (2.9)$$

Step 4: Corrective step

$$Step = (J_{gb}^T \times F_{gb}) \quad (2.10)$$

$$Step = Step / norm(Step) \quad (2.11)$$

Step 5: Compute the rate of change of quaternion using gyroscope data

$$\dot{q} = 0.5 \times (q \otimes [0, gyroscope]) - \beta \times Step^T \quad (2.12)$$

Step 6: Integration of quaternion rate to yield quaternion

$$q_t = q_{t-1} + \dot{q} \times Sample\ period \quad (2.13)$$

Notations and description of the equation can be found in details in the original paper [51].

Recent study has compared EKF, Mahony and Madgwick filters and have shown that three filters work equally in terms of accuracy [53]. However, computational time is

comparatively higher in EKF than Mahony or Madgwick filters. Another study has compared Mahony and Madgwick filter with basic AHRS filter and concluded that Madgwick filter outperform Mahony and basic AHRS filter in terms of accuracy [54]. When implementing the system for real-time data capturing, computational time is an important factor. Another important advantage in the Madgwick filter is that it compensates the magnetic disturbance where the metal structures around the ground fence is unavoidable. Considering the ease of implementation, execution time and the accuracy of the fusion algorithms, Madgwick filter was used to calculate IMU orientation in hitting analysis.

2.3. Hitting analysis in baseball game environment

Baseball has been playing professionally for over a century and game has been improved tremendously. One aspect is player performance. However, injuries during the game are also of a positive trend. Pitchers are more prone to injuries and biomechanics of pitching motion has been given a priority. Even though the ground conditions are different inside laboratory settings, throwing motion can be replicated inside confined laboratory settings by throwing towards a safety net. However, hitting motion needs a pitched ball towards batter from over 18 m away, which cannot be done unless otherwise a dedicated laboratory for baseball is implemented. This restricts hitting analysis for tee bat settings. Hitting a stationary ball is different from hitting a pitched ball in the context of perception and action

coupling [26]. This could be a major reason that biomechanical analysis of baseball hitting is comparatively lower.

Wireless sensors, specifically IMUs are being used in sports applications [55]. IMUs are small, and data can be collected wirelessly in real game setting without any movement restrictions. Moreover, IMUs are less costly compared to camera-based motion analysis systems and require less technical knowledge once the system is established. There is a high demand to use IMUs in sports motion analysis in real game settings. Though IMU is a promising motion analysis technique for baseball hitting, there are several downfalls due to which IMUs have not been used to analyze hitting motion in game environment.

Baseball hitting uses whole body as a sequence of segmental movements to generate power and timely hit a baseball in less than 500 msec. Therefore, hitting motion has broken down in to four major phases known as stance, wind-up, swing and follow through for comprehensive analysis. These phases are divided by three important events; foot-off, foot-on and impact (These phases and important events are described further in Chapter 3). These phases are generally identified by force plates and cameras in laboratory settings. IMUs only measure inertial measurements such as acceleration and angular velocity. It is difficult to predict movement patterns in baseball hitting without detecting these important hitting events.

Another drawback is the accurate measurement of the important hitting kinematics. IMUs have proven to be highly accurate in gait analyses [56]. However, baseball is a highly dynamic activity and IMUs should be validated for baseball hitting motion compared to an existing laboratory-based motion capture system before implementing in ground conditions.

IMU orientation should be calculated to measure segmental and joint angles. Madgwick filter was chosen as the fusion algorithm for orientation calculation. Most fusion algorithms have several tuning parameters that should be calculated prior to measurement. Madgwick filter has only parameter and that can be calculated by the initial calibration data. Further, Madgwick filter has shown high accuracy and have been used as a base algorithm to compare newly implemented algorithms [57]. Less computational cost is important for the possible real time calculations in future implementation and Madgwick filter has less computational cost than popular extended Kalman filter.

2.4. Research implementation

Commercial IMUs were used in the following experiments to implement a system that could be used to analyze hitting motion in a real game environment. Two IMUs attached on pelvis, and hand were used to detect foot-off, foot-on and impact events. Accuracy of the events were validated with the events measured by OMCS in the laboratory conditions. Additional IMU attached on thorax were used to calculate trunk and hand kinematics. Madgwick fusion

algorithm was used to derive IMU orientation. Finally, impact event was detected by hand IMU for pitched balls. Three separate experiments were conducted to investigate the usefulness of IMUs to analyze baseball hitting in a real game environment. Following chapters describe the experiments.

Chapter 3: Detection of the important hitting events using inertial measurement units

Chapter 4: Efficacy of inertial measurement units in analyzing baseball hitting motion

Chapter 5: Detection of the ball impact in pitched hitting condition using a hand worn inertial measurement unit

Chapter 3

3. Detection of the important hitting events using inertial measurement units

3.1. Introduction

Baseball hitting is a sequence of movements, starting from lower-body and then transfer the energy to trunk and upper body by rotation and translation of the respective body segments to generate high bat end velocity to hit a pitched ball. Motion of hitting occurs within about a second. Thus, it is required to capture the motion in millisecond intervals and divide into multiple phases to elaborate the biomechanical parameters (Figure 6). Previous research has divided the hitting into stance phase, wind-up phase, swing phase and follow through phase [3, 21, 23, 24, 59-62].

Stance phase: Hitter is waiting for the oncoming pitch delivered by the pitcher.

Wind-up phase: When pitcher starts moving to deliver the ball, hitter starts his movements simultaneously by shifting his weight to the rear/back leg and start moving forward while loading the energy by coiling the trunk.

Swing phase: Once hitter identified the ball trajectory and velocity that would reach in the strike zone, hitter starts unwinding the trunk and bring the bat head by rotating the upper body to contact with the pitched ball.

Follow-through phase: After ball contact with the bat, hitter decelerates the moving bat and upper body and prepare to run to the first base.

Some research has sub-divided the major phases to describe the hitting in detail [25].

However, the kinematic differences between sub phases does not differ significantly and thus four major phases were considered in this study.

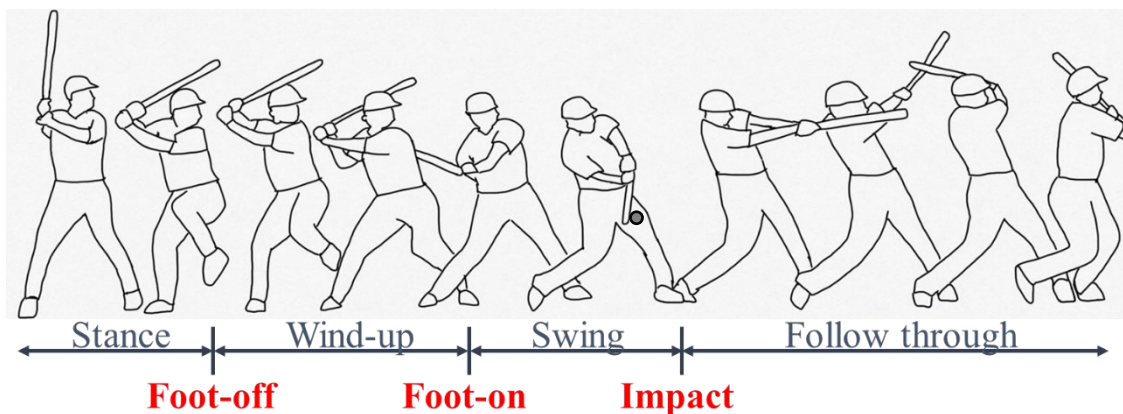


Figure 6: Phases of baseball hitting

Four major phases are identified by three key events namely, Foot-off, foot-on and bat-ball impact (Figure 7). In laboratory conditions, these phases are identified by force plate data (foot events) and cameras (impact). Different research groups have chosen different definitions to detect the key events depend on the equipment and their experimental outcome.

Foot-off

Foot-off event is generally detected by the ground reaction forces (GRF) of the force plate data when the experiment is conducted in the laboratory setting [21, 25]. Hitter lift his front foot while shifting his weight to the back foot. Front foot force data becomes zero at this point and be able to detect from force plate data. When the force plate data is not available, displacement of the toe marker has been used to detect the foot-off event [23].

Foot-on

Foot-on event does not have a specific definition in literature. Some research has taken foot on event at the time, the front foot is planted on the ground after the leg kick, detected by the force plate data [21, 27, 63, 64]. Ae and their research team have used the time when the force data exceeds 3% of the body weight to detect foot-on event [65]. Laughlin and their research group have defined the front foot support when the front foot force data surpasses 50% of the body weight [66]. Similar approach was taken by Fortenbaugh and his team to detect foot-on event which was termed as “weight-shift commitment” to understand the effect of the pitch types on ground reaction forces [62]. It was shown that hitters begin to transfer their weight to the front foot (surpasses 50% of the body weight) about 200 msec before bat contact with the ball, irrespective of the pitch type (Fast ball or change up). This is an important finding. A successful hit requires similar timing to transfer body weight to

the front foot and therefore the timing that surpasses 50% of the body weight was used as foot on event in this study.



Figure 7: Important events to be detected during hitting

Impact

Bat-ball impact can be detected by high-speed video cameras or by monitoring the displacement of the reflective marker attached on the ball. In baseball batting, ball is in contact with the ball about 1.5 msec [67, 68]. Most of the previous research have used 250 Hz or less sampling rate. Therefore, exact time frame of the bat-ball contact could not be detected. Thus, impact time is taken as the frame before the bat-ball collision [21, 23-25, 63, 66, 67].

It is difficult to setup force plates in a real ground to detect foot events (Foot-off and foot-on). Synchronizing cameras with IMU system increase additional cost and effort to detect impact event. Direction of the propulsive force at foot off and breaking force at foot on towards pitcher's direction has a detectable shift. It was hypothesized that accelerometer

data of the IMU attached on pelvis could detect the directional differences of these forces. Furthermore, hitters keep increasing the hand velocity until bat ball impact [69]. Thus, our second hypothesis was that acceleration of the IMUs attached on the hands could possibly have local peaks near the bat-ball impact event. Results were validated with an optical motion capture system (OMCS).

3.2. Methodology

3.2.1. Participants

Ten male baseball players from University of Miyazaki baseball team participated in the study (Mean age, 20.9 (standard deviation = ± 1.1) years, mean height, 1.7 (± 0.1) m, mean body mass, 71.3 (± 6.4) kg). Purpose and outcome of the study was explained to the participants and a written informed consent was taken prior to data collection. Participants were classified into two groups depending on their wind-up style, *kick hitting* or *glide hitting*.

3.2.2. Hitting styles

Kick hitting (KH) is referred to the hitters who has higher knee bend during lifting off the front foot at foot-off event and plant the front foot during weight transfer (Figure 8 (a)). Some players lean back to the back foot while partially lifting the front foot and may rest the front foot before transferring the weight to front foot during forward movement before swinging the bat. This is referred as glide hitting (GH) (Figure 8 (b)).



(a) Kick hitting



(b) Glide hitting

Figure 8: Different hitting styles based on front foot movement

After self-selected warming up, each participant hit a baseball suspended on a tee-pole five times from their natural hitting style. After performing first 5 trials, participants were given enough time to get accustomed to the other hitting style. They performed five more hitting off a tee pole in the other hitting style. Not less than 30 seconds were given between each swing. Hitting motion was recorded from IMUs and OMCS simultaneously.

3.2.3. Instrumental setup

3.2.3.7. *IMUs*

Three wireless IMUs (MyoResearch® model 610, Noraxon Inc., Scottsdale, AZ, USA) were attached on the pelvis and on each hand. Each IMU consisted with a tri-axial accelerometer ($\pm 157.0 \text{ ms}^{-2}$), tri-axial gyroscope ($\pm 2000 \text{ deg.s}^{-1}$), and a tri-axial magnetometer (± 1.9 Gauss) (Figure 9).

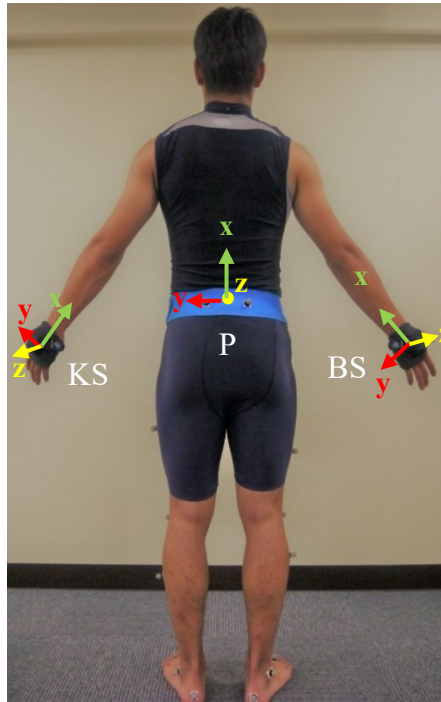


Figure 9: IMU attachment on body segments

IMU on the pelvis was directly attached on the skin using a double-sided tape and further secured with an elasticized bandage. IMUs on the dorsal side of each hand were secured using neoprene tapes. local coordinates of the IMUs were aligned with the anatomical landmarks. Wireless receiver was connected to a laptop computer and data recorded at 200 Hz sampling rate in each swing was directly stored in the hard disk. Bony landmarks with less muscles were selected to attach the IMUs. This will reduce the skin and muscle artefacts during swing motion.

3.2.3.8. OMCS

10 infrared cameras (Vantage-V8, Vicon Motion Systems Ltd., UK) and two force plates (Advance Mechanical Technology Inc., MA, USA) were employed in this study. Sampling rate was set to 250 Hz for cameras and 1000 Hz for force plates. Global coordinates of the OMCS were set denoting the landmarks of a baseball field. Y-axis was set towards the pitcher's direction and Z-axis was vertically oriented upwards. X axis was derived from the cross product of the Y and Z axes (Figure 10).

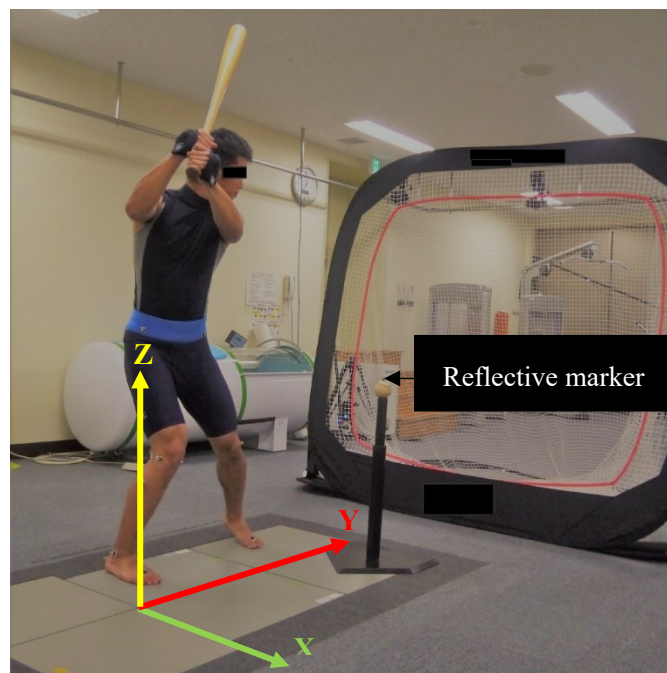


Figure 10: Hitting trials off a tee pole. Global reference system is denoted in XYZ

Two reflective markers were attached on left and right posterior iliac spines centering the pelvis IMU. displacement of the center point of the 2 markers were used to evaluate the pelvis motion towards pitcher. A reflective marker was attached on the ball suspended on a

tee pole to detect bat-ball impact event. Participants were instructed to keep their legs apart on each force plate during the stance.

3.2.4. Data processing

Data processing was performed using separate scripts written in MATLAB® for IMUs and OMCS.

3.2.4.7. Detection of the key events by OMCS

GRF of the front foot force plate and marker displacement attached on the ball were used to detect foot events and impact timing respectively. High frequency noise in the force plate data was filtered out using a 4th order, low-pass Butterworth filter with 75 Hz cut off frequency. Foot-off was defined at the time when the front foot GRF becomes zero [21, 63]. when the front foot was not completely lifted in GH style, local minimum was used as foot-off event. Foot-on event was taken as the time when the body weight surpassed 50% of the participant's bodyweight [62, 66]. Displacement data of the reflective marker attached on the ball was used to detect the impact time [24, 70].

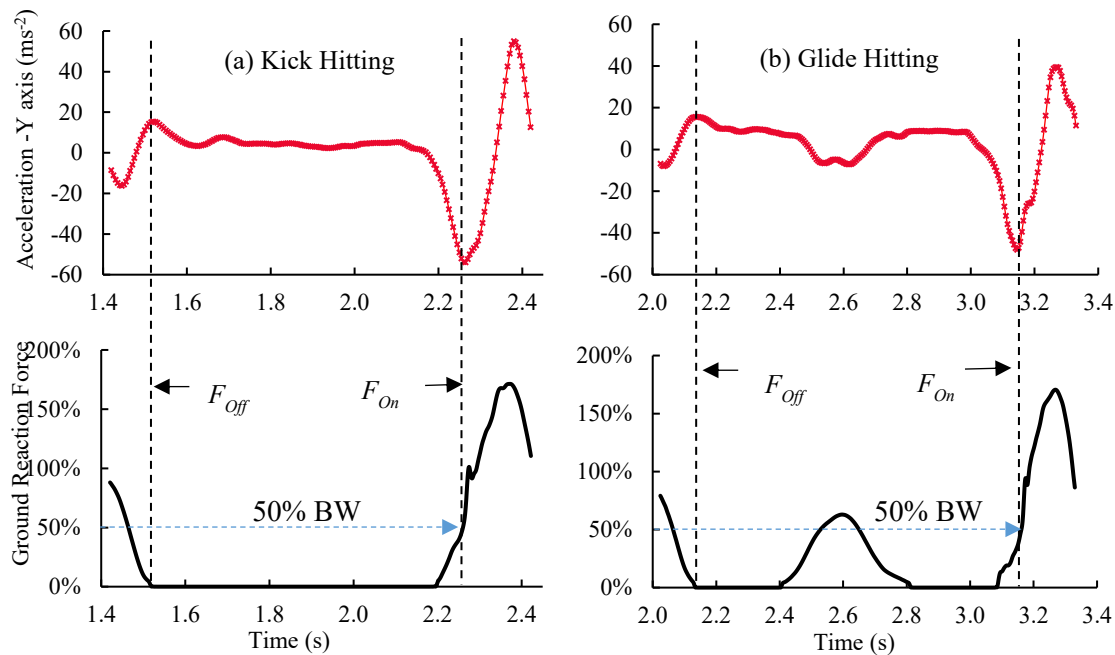


Figure 11: Typical graphs of foot event comparison. Top graphs are pelvis acceleration towards Y direction and bottom graphs are the respective force plate data

3.2.4.8. Detection of the key events by IMUs

Local acceleration data of the IMU placed on the pelvis was transformed into the global coordinates and the acceleration to the direction of the pitcher (global Y-axis) was used to detect foot-off and foot-on events. Before each hitting trial, participant was asked to stand still facing the home plate. This static position kept the local y-axis of the pelvis IMU parallel with the global Y-axis. Initial orientation was set to zero at the static pose. Euler angles calculated from the proprietary software (MyoResearch®) was then used to calculate the rotation matrix from which the acceleration data were transformed from IMU local

coordinates to global coordinates (Appendix A). A gaussian convolution filter with window size 10 was used to smooth the acceleration profile and amplify the signal to be able to detect the local peaks from the algorithm written in MATLAB. First positive peak was defined as the foot-off time while foot-on time was defined as the minimum acceleration (negative peak) towards the pitcher's direction (Figure 11).

Acceleration data in local coordinates of the knob side (KS) and barrel side (BS) hands were used to locate the impact time. Fourth order, zero-lag, low pass Butterworth filter was used with the cut off frequency of 20 Hz to remove high frequency noise. Negative acceleration peak in the local x-axis in each hand was defined as the impact time (Figure 12).

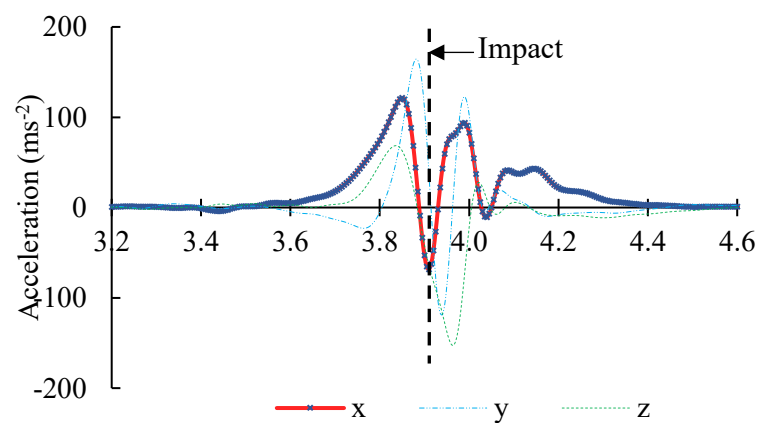


Figure 12: Impact time detection using local acceleration of the hand IMU. vertical broken represents impact time detected by OMCS

Peak of the signal does not necessarily be a data point. Therefore, the peak value was detected by calculating the rate of change of acceleration and interpolating data where rate of change of acceleration reached zero.

3.3. Statistical analysis

One trial was excluded due to poor data recording. Total of 99 hitting trials (KH = 49, GH = 50) were used in the analysis. Timing of the key events detected by IMUs and OMCS were compared. Root mean square error was calculated to quantify the accuracy of the timing. Intraclass correlation coefficient (ICC; a two-way mixed model for absolute agreement) was used to measure the reliability of the event detection. Mann-Whitney U test was used to compare the time differences in KH and GH styles. In addition, detection of the impact time in KS and BS were also compared. $P < 0.05$ was considered statistically significant. Statistical package for the social sciences (SPSS; version 21.0, IBM Corp, Tokyo, Japan) was used in the statistical analysis.

3.4. Results

3.4.1. Foot-off and foot-on events

Foot-off and foot-on events could be closely detected in both hitting styles by the acceleration data towards the pitcher's direction using the IMU placed on pelvis. $ICC > 0.99$ showed an excellent reliability to detect the foot event using IMU compared to the OMCS.

RMSE of the foot-off was 0.024 s in both hitting styles. For foot-on, Mann-Whitney U test revealed that GH (RMSE = 0.029 s) detected more accurately than KH (RMSE = 0.032 s) with p value less than 0.001.

Table 1: Mean error and standard deviation (SD) root mean square error (RMSE), and intraclass correlation coefficient (ICC) of the pelvis peak position detected at the foot on event

Hitting Style	Mean (SD) (s)	RMSE (s)	ICC (CI, 95%)
Overall	0.000 (0.053)	0.053	0.996 (0.994, 0.997)
Kick Hitting	0.008 (0.059)	0.059	0.995 (0.991, 0.997)
Glide Hitting	-0.008 (0.047)	0.047	0.997 (0.995, 0.998)

Pelvic position initially moved opposite to the pitcher when leaning back and gradually started moving towards the pitcher's direction reaching the peak when the body weight is transferred on the front foot. Foot-on time coincided with the peak pelvic position towards pitcher's direction with overall RMSE of 0.053 s (Table 1).

3.4.2. Impact event

Acceleration along the local x-axis of the KS and BS hands corresponded to the impact time detected by OMCS (ICC = 1.00). RMSEs of the KS and BS hands were 0.009 s and 0.011 s, showing a significant close detection from the KS hand ($p = 0.001$) (Table 2).

Table 2: Mean error and standard deviation (SD), root mean square error (RMSE), and intraclass correlation coefficient (ICC) with 95% confident intervals (CI) at the events detected by inertial measurement units

Event	Hitting Style	Mean (SD) (s)	RMSE (s)	ICC (CI, 95%)
Foot-off	Overall	0.005 (0.024)	0.024	0.999 (0.998, 0.999)
	Kick Hitting	0.014 (0.019)	0.024	0.999 (0.996, 1.000)
	Glide Hitting	-0.004 (0.024)	0.024	0.999 (0.998, 0.999)
Foot-on	Overall	0.006 (0.030)	0.031	0.999 (0.998, 0.999)
	Kick Hitting	0.008 (0.032)	0.032	0.998 (0.997, 0.999)
	Glide Hitting	0.005 (0.029)	0.029	0.999 (0.998, 0.999)
Impact (KS)	Overall	0.000 (0.009)	0.009	1.000 (1.000, 1.000)
Impact (BS)	Overall	-0.004 (0.011)	0.011	1.000 (1.000, 1.000)

3.5. Discussion

Baseball hitting is a complex motion that requires whole body movement in a very short amount of time. To analyze biomechanical parameters of hitting, it is important to separate the total motion into main phases by key events. Therefore, accurate identification of the key events is essential. This study showed that the foot-off, foot-on and impact events could be detected using IMUs attached on pelvis and hands. Reliability of detecting the key event was excellent for each event ($ICC > 0.99$) compared to the conventional methods used in OMCS. Foot events were detected within 0.032 s of RMSE while impact error was 0.009 s

under tee-batting conditions, comparatively low when considering the total swing time. Mean swing time (foot-on to impact) in the current study was 0.163 s which is similar to the values presented in previous studies (range: 0.166 – 0.201 s) [62, 66].

3.5.1. Foot events

Propulsive and braking forces of the front and back foot during the bat swing have a significant effect on trunk motion towards the pitcher's direction [3, 66]. Moreover, trunk movement towards the pitcher's direction (Y-axis) is important to adjust the bat swing for different pitch locations [71] and different pitch speeds [72]. As hypothesized, linear motion of the trunk showed correlation with the foot-events and thus trunk linear acceleration could be used to closely detect the foot events.

3.5.2. Impact event

Both KS and BS hands could closely detect the impact time in which RMSE bounded to 11 msec, which is closely equivalent to 2 data points when data is collected at 200 Hz. local x-axis of the IMU was approximately parallel to the direction of the impact, where hitter tries to hit the ball with maximum efficiency, maintaining the barrel almost perpendicular to the direction of impact. Since x-axis was in the opposite direction to the impact, a minimum peak could be observed. Some hitters release their BS hand just after the bat-ball impact.

Furthermore, grip strength of the KS hand is higher than BS in baseball hitting [73]. This could be the reason for high accuracy of impact time detection in the KS than BS hand.

3.5.3. Limitations

Main limitations in this study were bound with the specification of the IMUs. Maximum sampling rate of the IMUs used in this study was 200Hz which measures data in 5 msec intervals. Ball is in contact with the bat less than 1.5 msec and thus it was difficult to directly measure the impact time [67]. Therefore, the central difference method was adopted to calculate rate of change of acceleration to detect the impact time [74]. In addition, hand acceleration exceeded the measurement range of the IMU. A higher sampling rate over 1000 Hz and higher measurement range is required to increase the accuracy [2].

It is difficult to fully secure the IMUs attached on the hands which would restrict the gripping the bat. Therefore, skin artefacts were present and relative movement may have changed the orientation slightly. Moreover, OMCS was incorporated to validate the IMU measurements and thus, this study was limited to tee-batting. Hitting a stationary ball is difficult than hitting a pitched ball in terms of perception-action coupling [26]. Further validation is necessary for the proposed method to be used in live pitching conditions.

3.5.4. Summary

This study demonstrated a method to detect important events in baseball hitting using IMUs.

An IMU attached on pelvis could detect foot-off and foot-on events while IMU attached on the dorsal side of the knob side hand could closely detect the impact time. Adequate validity and excellent reliability demonstrated the usefulness of the IMUs to analyze baseball hitting.

Chapter 4

4. Efficacy of inertial measurement units in analyzing baseball hitting motion

4.1. Introduction

Hitting a pitched baseball require excellent coordination of the body segments [70]. A fast ball reaches the home plate within 0.5 s and thus high skill is required to detect the speed and trajectory of the ball and (Perception) and timely translate and rotate body segments (action) to bring the bat to the ball with high velocity [75]. Outcome of the successful hit is determined by the speed and trajectory of the batted ball. Good trajectory can land the ball safely between fielders without getting out by a direct catch. Even in lower trajectories where ball hit the ground in the infield can still be a base hit if the ball has enough velocity to pass through the fielders or the fielders to make errors. Excellent speed and trajectory of the batted ball will land out of the fence called a 'home run', which is the single highest achievement in baseball hitting.

Rotational motion along the longitudinal axis of the body is important in increasing swing speed [71]. Skilled baseball players show higher axial trunk angular velocity than low skilled players [76]. Also, trunk strength training can significantly improve swing speed [77, 78]. Trunk rotation plays a significant role in hitting performance. However, incidence of

abdominal muscle injuries is increasing. About 50% of abdominal muscle injuries in baseball are accounted to during hitting motion and majority of them are occurred in the internal/external oblique muscles [4]. Oblique muscles stabilize the trunk movements, evidently trunk rotation. Oblique muscles are activated greater than 100% of its maximum voluntary contraction during swing phase and follow through [18]. Peak lumbar spine rotation may contribute to lumbar disk herniation [63]. Thus, evidence of biomechanics may help reduce abdominal injuries while enhancing trunk motion in baseball hitting.

IMUs can be attached on player's body segments and kinematic data can be collected in outdoor environment, which is very difficult in conventional OMCS. However, IMUs have not been validated to measure trunk kinematics in baseball hitting. Therefore, aim of this study was to evaluate the validity and reliability of the IMUs in analyzing trunk kinematics. It was hypothesized that IMUs with 1000 Hz sampling rate can be used in assessing the coordination of hitting. Therefore, hand kinematics were also observed.

4.2. Methodology

4.2.1. Participants

Eight male baseball players (Mean age, 19.9 (standard deviation = ± 1.4) years, mean height, 1.7 (± 0.1) m, mean body mass, 69.0 (± 10.9) kg) from University of Miyazaki baseball club voluntarily participated in the study. All participants had no history of musculoskeletal

disorders and had more than 10 years of playing experience. Experimental protocol and expected outcomes were explained to the participants and a written informed consent was obtained prior to data collection. Motion analysis laboratory of the rehabilitation center in University of Miyazaki hospital was used in this experiment.

4.2.2. Instrumental setup

Three IMUs were incorporated (sampling rate of 1000 Hz, SS-MS-HMA200G60 (accelerometer (± 200 G, $G = 9.81 \text{ ms}^{-2}$), gyroscope ($\pm 6000 \text{ }^\circ\text{s}^{-1}$), magnetometer (± 10 gauss)), size: 36 mm (width) \times 53 mm (length) \times 11 mm (depth), weight: 32 g, Sports Sensing Co., Ltd., Fukuoka, Japan) in the current study (Figure 13). Each IMU consisted with an internal memory to record data. A wireless transceiver was connected to the computer from which all the IMU were synchronized for data recording. Fully charged IMUs were kept for 10 minutes after switched on to allow the sensors to achieve steady state. Accelerometer and magnetometer were calibrated before data collection. Calibration procedure is explained in Appendix B.

After calibration, IMUs were attached on thorax, pelvis, and hand segments. Thorax IMU was attached between the manubrium and xiphoid process of the sternum. Pelvis IMU was attached between the left and right posterior iliac spines. Thorax and pelvis IMUs were attached such that x-axis corresponded to the medio-lateral direction and y-axis

corresponded to the longitudinal towards the upwards direction based on the anatomical landmarks of the respective segment. Hand IMU was attached on the dorsal side of the leading hand (knob side hand when the bat was held) over the batting glove using a double-sided tape and further secured with an elasticized bandage. y-axis of the hand IMU was aligned with the long axis towards the proximal direction of the hand.

4.2.3. Data collection



Figure 13: Inertial measurement unit used in the current study. 500-yen coin was kept besides for size comparison

After self-selected warmup exercises, each player hit a baseball suspended on a tee-pole 10 times with resting time not less than 30 s were given between each swing. Players were allowed to adjust the tee-pole to their preferable height. Before each hitting measurement, players were instructed to stand still for 5 s while facing the home plate (static pose). Static pose was used to determine the initial orientation and to calculate the gyroscope bias. Data stored inside the IMU memory were transferred to a computer at the end of the session.

4.2.3.1. Calculation of the kinematics using IMU data

A script written in MATLAB (version R2017b, Mathworks®, Natick, MA, USA) was used to calculate IMU orientation. Mean angular rates of the static pose was deducted from gyroscope data in each trial to remove initial gyroscope bias. Gyroscope values in each axis were set to zero if the value was less than three times of the standard deviation at the static pose [79]. Acceleration and angular rates were then filtered using a fourth order, low pass Butterworth filter with cutoff frequency of 15 Hz. Madgwick filter was incorporated to calculate orientation of the IMUs attached on each body segment [51]. Orientation was represented in unit quaternion. Quaternion has several advantages over Euler angles and rotation matrix among lower computational load [80]. Basics of the quaternions is given in Appendix C. quaternion ($q(t)$) in each IMU was represented with respect to a common global coordinate system derived by the gravity and magnetic north vectors.

Static quaternion (q_{stat}) was calculated from the last 0.5 s of the static pose. Segmental orientation ($q_{seg}(t)$) was then represented with respect to the q_{stat} using the following equation:

$$q_{seg}(t) = q(t) \otimes q_{stat}^* \quad (4.1)$$

Where q^* represents quaternion conjugate while \otimes represents quaternion multiplication.

YXZ Euler sequence was used to calculate angular displacement in each segment (Appendix

C). Both thorax and pelvis had highest range of motion in the longitudinal axis which

represented by y-axis and thus YXZ sequence was used to prevent gimbal lock [81, 82].

Thorax and pelvic orientation were then used to calculate spine angles (Figure 14). Joint coordinate system (JCS) was used to calculate spine angles recommended by the international society of biomechanics [83, 84]. JCS was initially proposed to knee joint and more generalized algorithm has been introduced to apply in other joints [85]. Generalized definition of the joint axes are given below.

Flexion axis: Axis of the segment coordinate system, oriented in the mediolateral direction (unit vector $\hat{\mathbf{f}}$)

Longitudinal axis: Axis of the distal segment coordinate system, oriented in the longitudinal direction (unit vector $\hat{\mathbf{l}}$)

Third axis: Third axis (floating axis) is calculated as the cross product of the longitudinal and flexion axes (unit vector $\hat{\mathbf{t}} = \hat{\mathbf{l}} \times \hat{\mathbf{f}}$)

Proximal and distal segments can then be defined relative the inertial system. Suffices p and d denote proximal and distal segments respectively.

$$\hat{\mathbf{e}}_1 = -\mathbf{f}_p \quad (4.2)$$

$$\hat{\mathbf{e}}_3 = \mathbf{l}_d \quad (4.3)$$

$$\hat{\mathbf{e}}_2 = \left(\frac{\hat{\mathbf{e}}_3 \times \hat{\mathbf{e}}_1}{|\hat{\mathbf{e}}_3 \times \hat{\mathbf{e}}_1|} \right) * A \quad (4.4)$$

Where, $A = -1$ if $(\hat{\mathbf{e}}_3 \times \hat{\mathbf{e}}_1) \cdot \mathbf{t}_d < 0$ and $((\hat{\mathbf{e}}_3 \times \hat{\mathbf{e}}_1) \times \hat{\mathbf{e}}_3) \cdot \mathbf{f}_d > 0$, 1 otherwise

Three angles of the rotation in the 3D joint were calculated as follows:

$$\text{Flexion angle} = \cos^{-1}(\hat{e}_2 \cdot \hat{t}_p) * \text{sign}(\hat{e}_2 \cdot \hat{l}_p) \quad (4.5)$$

$$\text{Lateral flexion angle} = \cos^{-1}(\hat{r} \cdot \hat{l}_d) * \text{sign}(f_p \cdot \hat{l}_d), \text{ where } \hat{r} = \left(\frac{f \times \hat{e}_2}{|f \times \hat{e}_2|} \right) \quad (4.6)$$

$$\text{Axial rotation angle} = \cos^{-1}(\hat{e}_2 \cdot \hat{t}_d) * \text{sign}(\hat{e}_2 \cdot \hat{f}_d) \quad (4.7)$$

Segmental angular velocities could be directly derived from the gyroscope data. Spine angular velocity was derived by calculating first derivative of the time dependent spine angles.

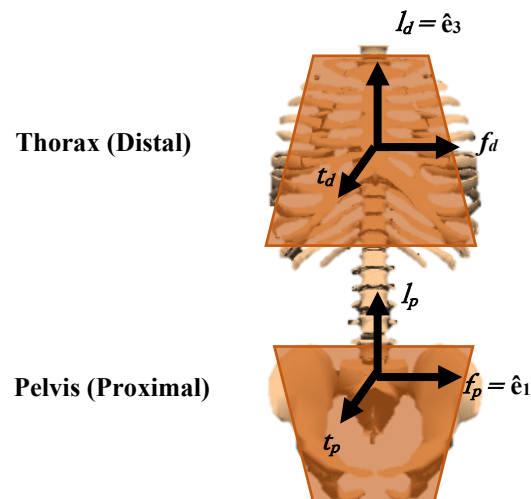


Figure 14: Trunk segments with respective local coordinates

4.2.3.2. Estimation of hitting events and hand kinematics

Key events of the hitting sequence were detected by IMUs as described in the previous study (Figure 15 (a)). Hitting events were obtained to describe the hitting motion and coordination of the segments during the baseball swing.

Acceleration of the IMU attached on the hand was used to derive the resultant linear velocity (Figure 15 (b)). Acceleration data were transformed to global coordinates system and gravity vector was removed before calculating the velocity. A threshold value of 0.1 G ($G = 9.81 \text{ ms}^{-2}$) was used to recognize the initial hand movement during the forward swing phase.

4.2.3.3. Kinematic data validation with OMCS

Trunk and hand kinematics calculated from IMUs were compared with OMCS (sampling rate of 250 Hz, 13 cameras, Vicon motion Systems Ltd, Oxford, UK). An active wand was used to calibrate the cameras with residual error less than 0.2 mm. Data were captured in IMUs and OMCS simultaneously by synchronizing both systems using a 5 V pulse trigger.

An I-shaped acrylic plate (thickness, 3 mm; weight, 14 g) with 4 reflective markers were attached on top of the IMUs attached on thorax and pelvis (Figure 16 (a-c)).

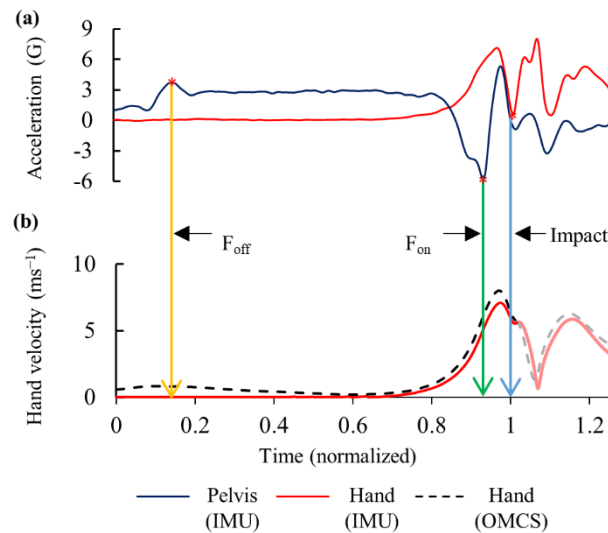


Figure 15: Important events detected by IMUs (a) and hand velocity graphs from both systems

IMU-acrylic plate unit was attached on players body segment using a double-sided tape and further secured with elasticized bandage. Marker trajectories tracked by OMCS were used to construct local coordinates of each segment, that were corresponded with the local coordinates of the respective IMUs. A reflective marker was attached on the IMU attached on the player's hand to track the hand motion (Figure 16 (d)). Another marker was attached on the ball to detect bat-ball impact from OMCS.

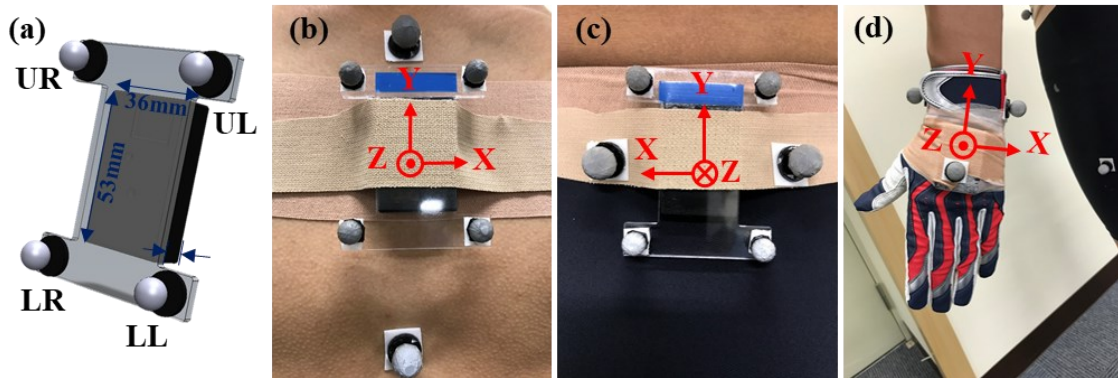


Figure 16: positioning of the inertial measurement units (IMUs) on body segments.

(a) IMU attached on acrylic plate, (b) IMU on thorax, (c) IMU on pelvis, (d) IMU on hand

Marker trajectories were low pass filtered using a 4th order Butterworth filter with the cut of frequency of 20 Hz. local coordinates of the thorax and pelvic segments were constructed using the markers attached on the acrylic plates using following equations.

$$X = \frac{([LL + UL] \div 2 - [LR + UR] \div 2)}{\|([LL + UL] \div 2 - [LR + UR] \div 2)\|} \quad (4.8)$$

$$Z = X \times \frac{([UR + UL] \div 2 - [LR + LL] \div 2)}{\|([UR + UL] \div 2 - [LR + LL] \div 2)\|} \quad (4.9)$$

$$Y = Z \times X \quad (4.10)$$

where, LL: lower left marker, UL: upper left marker, LR: lower right marker, UR: upper right marker. Three dimensional vectors of X, Y and Z are written in column matrix to generate the respective rotation matrix [X, Y, Z]. Angular displacement of each segment was then calculated by first converting the rotation matrix into quaternion format and following the same procedure described to calculate orientation of IMUs. Segmental angular velocity from the quaternion derived from the marker data were calculated by following equations.

$$\dot{q}_{seg} = \frac{q_{seg}(t+1) - q_{seg}(t-1)}{2\Delta t} \quad (4.11)$$

$$\omega' = 2 \left(q_{seg}^*(t) \otimes \dot{q}_{seg} \right) \quad (4.12)$$

where, Δt is the time stamp between 2 data points (4 ms). $\omega' = [\omega_0, \omega_1, \omega_2, \omega_3]$ was represented in quaternion format and thus angular velocity $\omega = [\omega_1, \omega_2, \omega_3]$ [86]. A fifth-order median filter was used to reduce noise in angular velocity acquired from both systems. Trajectory of the marker attached on the hand was used to derive the linear velocity. Displacement of the reflective marker attached on the ball was visually monitored to identify the bat-ball impact [69].

4.3. Statistical analysis

Swing period was defined from the hand started moving to bat-ball impact. One trial was excluded due to data loss in the IMU data therefore, 79 trials were included in data analysis.

Angular displacement and angular velocity were the parameters considered to evaluate in the thorax, pelvis and spine. Accuracy of the angular displacement curves obtained from IMUs and OMCS were analyzed by calculating averaged root mean square error (RMSE).

An RMSE $< 5^\circ$ was considered excellent accuracy, between 5° and 10° was considered a good estimation [87, 88]. Mean absolute error (MAE) was used to estimate the accuracy of the angular velocity. MAE was represented as a percentage of the maximum angular velocity during the swing period. Reliability of IMUs were evaluated by intraclass

correlation coefficient (ICC; a two-way mixed model for absolute agreement) was calculated using the statistical package for the social sciences software (version 22.0, IBM Corp., Tokyo, Japan). Angular displacement at the impact was used as reliability measurement while peak value was used in angular velocity data. An ICC < 0.5 was considered poor reliability, between 0.5 To 0.75 was considered moderate, between 0.75 and 0.9 was considered good and > 0.9 was taken as excellent reliability [89]. Agreement between the measurement systems were evaluated using Bland-Altman analysis [90]. Moreover, peak hand velocity and impact time difference between two measurement systems were also compared.

4.4. Results

4.4.1. Description of the baseball swing using IMUs

During knee flexion at the foot-off event, pelvis is flexed, but thorax was kept steady to maintain the gaze towards pitcher at the wind-up phase. Thorax started rotating counterclockwise, more than that of pelvic rotation, creating a coil like effect in the spine to generate rotational load just before the weight transfer at the front foot during foot-on event (Figure 17).

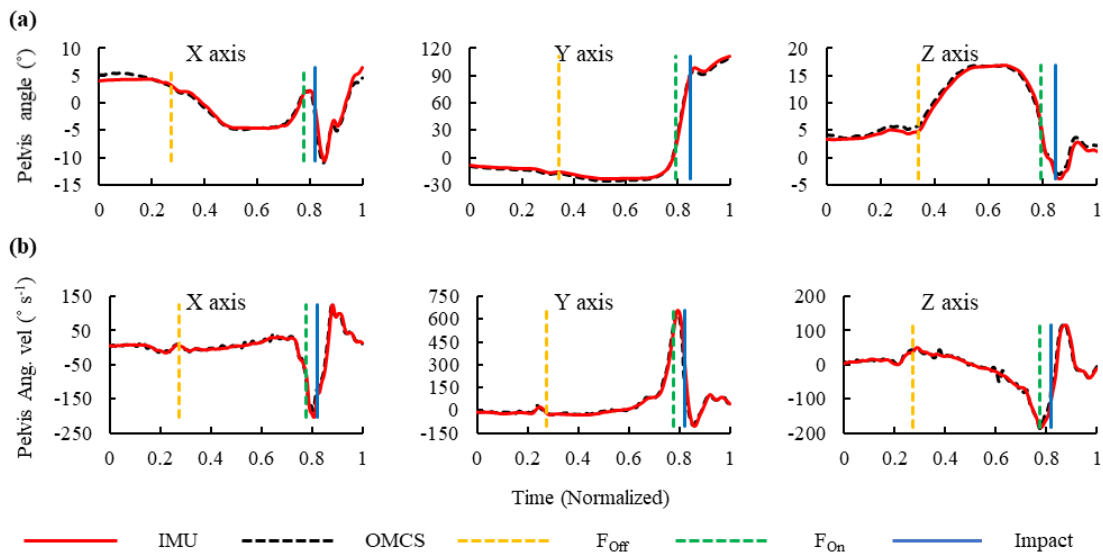


Figure 17: Pelvis angle and angular velocity calculated by inertial measurement unit (IMU) and optical motion capture system (OMCS). vertical lines in the graph represent the key events

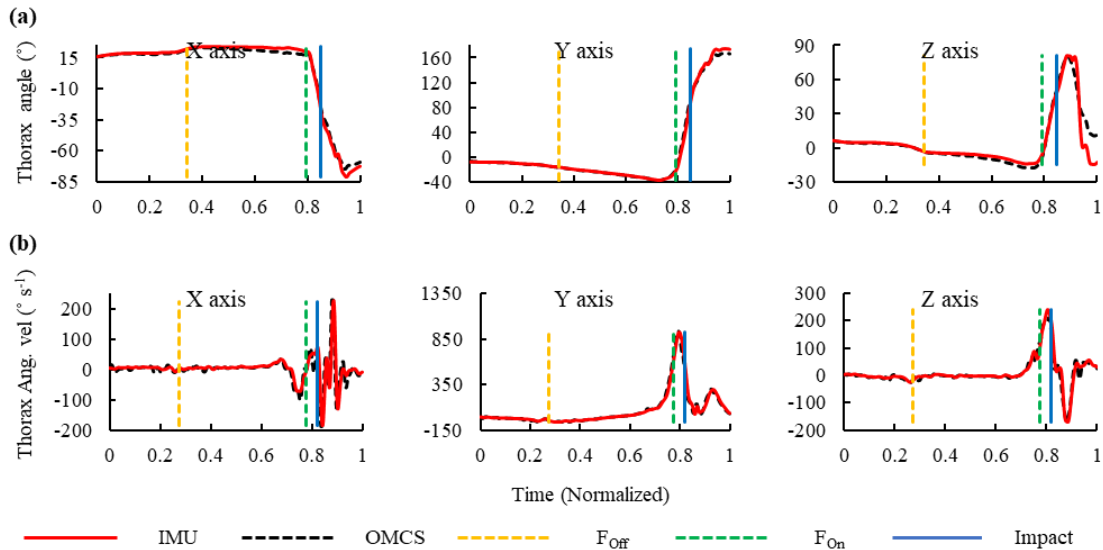


Figure 18: Thorax angle and angular velocity calculated by inertial measurement unit (IMU) and optical motion capture system (OMCS). vertical lines in the graph represent the key events

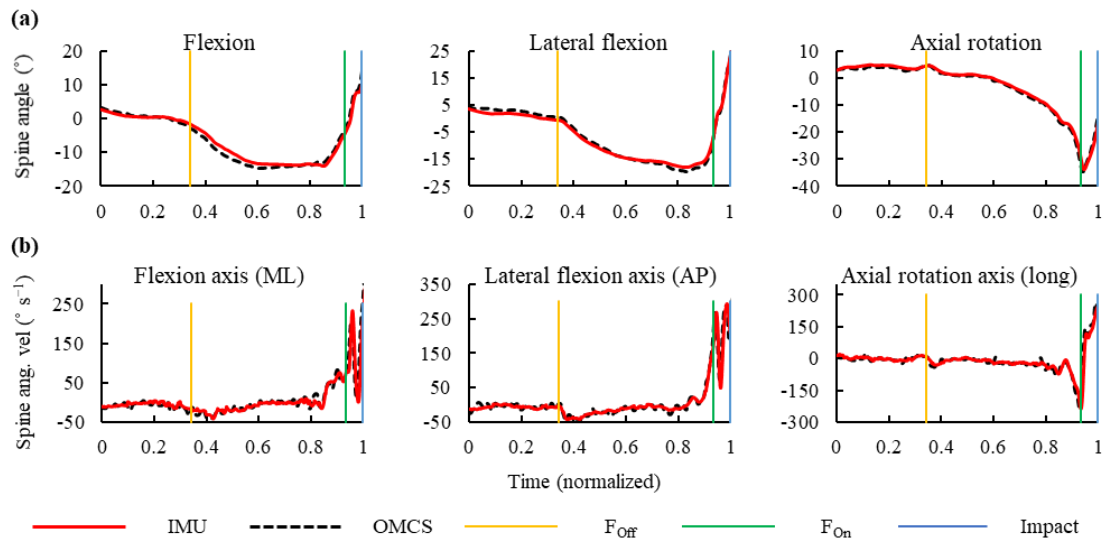


Figure 19: Spine angle and angular velocity detected by inertial measurement units (IMUs) and optical motion capture system (OMCS). vertical lines in the graph represent the key events

Pelvis started rotating clockwise before the foot-on event storing more rotational power and sudden increase of thorax angular velocity could then be observed before the impact (Figure 18). Thorax angular velocity peaked before the impact followed by thorax, revealing the concept of kinetic chain [2]. Average windup phase (foot-off to foot-on) was 1.422 (SD = 0.473) s, and swing phase (foot-on to impact) was 0.153 (0.023) s.

4.4.2. Validity and reliability of the IMUs

Validity of the IMUs have shown excellent when compared with OMCS. RMSE was 5° or less in trunk angular displacements (Table 3). For angular velocities, MAE was $\leq 5\%$ in the trunk segments and spine joint.

Table 3: Root mean square error (RMSE) and mean absolute error (MAE) of the trunk segmental and spine angles

Segment/ joint	Axis	RMSE (°) (Angular displacement)	MAE (%) (Angular velocity)
Thorax	x	2.16	5.06
	y	3.78	3.66
	z	2.64	2.37
Pelvis	x	1.57	5.58
	y	1.94	1.59
	z	1.36	2.13
Spine	Flexion (ML) ¹	2.69	4.14
	Lateral flexion (AP) ²	1.83	1.37
	Axial rotation (long) ³	1.49	4.48

Angular displacement at impact and peak angular velocities had excellent reliabilities with an ICC of > 0.950 . Bland-Altman analysis showed mean bias of $\pm 2.5^\circ$, and the limit of agreement was within $\pm 10^\circ$ in the angular displacements at the impact except spine flexion angles (Figure 20).

Hand velocity at peak and at impact were $7.94 (1.14) \text{ ms}^{-1}$ and $4.70 (0.83) \text{ ms}^{-1}$ respectively. MEA and ICC at peak and impact were 7.18%, 0.920 and 8.68%, 0.905. Mean error at the detection of impact $0.007 (0.004) \text{ s}$ and RMSE was 0.008 s with 1.000 of excellent reliability.

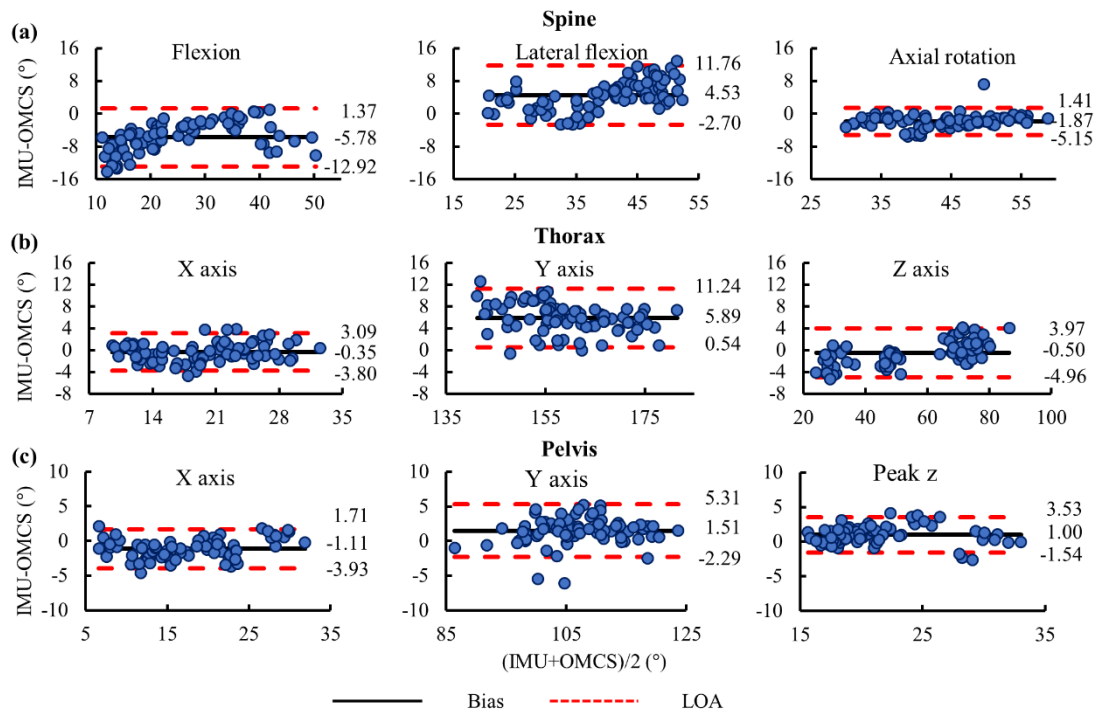


Figure 20: Bland-Altman graph of the (a) Spine, (b) Thorax and (c) Pelvis angles at impact

Table 4: Mean, bias and limit of agreement (LOA in upper and lower bounds (UB, LB)) and the corresponding intraclass correlation coefficient of the segmental and spine angles at impact and peak angular velocity

Segment/Joint	Axis	Angles at Impact (°)				Peak Angular Velocity (°s ⁻¹)			
		Mean (SD)	Bias	LOA (UB, LB)	ICC	Mean (SD)	Bias	LOA (UB, LB)	ICC
Thorax	x	-21.2 (4.8)	-1.87	(2.18, -5.93)	0.909	237.5 (156.8)	25.02	(129.42, -79.38)	0.955
	y	88.6 (11.5)	-1.06	(6.55, -8.67)	0.969	973.9 (248.0)	-0.21	(100.20, -100.62)	0.988
	z	40.5 (9.3)	-2.22	(5.81, -1.36)	0.976	423.9 (117.9)	10.5	(68.18, -47.18)	0.981
Pelvis	x	-1.0 (6.2)	-2.53	(0.42, -5.48)	0.951	145.5 (49.5)	8.01	(20.73, -4.72)	0.989
	y	79.2 (13.2)	-0.63	(3.26, -4.53)	0.994	643.0 (49.7)	6.34	(19.23, -6.54)	0.991
	z	-13.7 (8.2)	-1.54	(1.56, -4.64)	0.980	423.9 (117.9)	2.62	(9.51, -4.28)	0.998
Spine	Flexion (ML) ¹	0.0 (7.4)	-8.66	(-0.01, -17.30)	0.632	346.5 (172.5)	8.76	(101.45, -83.93)	0.982
	Lateral flexion (AP) ²	29.8 (7.6)	1.42	(6.81, -3.97)	0.953	339.7 (110.3)	25.45	(91.64, -40.73)	0.958
	Axial rotation (long) ³	2.3 (8.2)	-1.08	(1.60, -3.76)	0.988	705.5 (410.6)	43.9	(185.17, -97.37)	0.988

¹ ML: Medio-lateral axis, ² AP: Antero-posterior axis, ³ long: Longitudinal axis.

4.5. Discussion

4.5.1. Hitting characteristics

Characteristics of hitting motion could be well understood using IMUs with 1000 Hz sampling rate, attached on thorax, pelvis and hand. Sequential motion from proximal to distal segments during baseball hitting was indicated by IMU data [22]. Timing of the peak velocity differences of pelvis to thorax as well as thorax to hands were 12 msec and 8 msec, indicating 2-3 data points when data is captured at 250 Hz sampling rate (Figure 21).

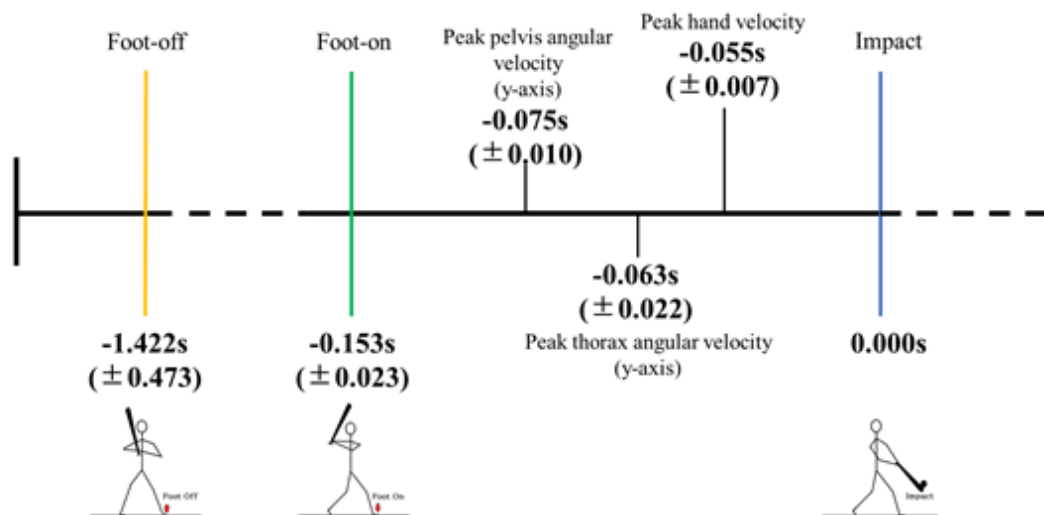


Figure 21: Coordination of the key events and peak kinematic parameters of the trunk and hand segments

Most of the past research have used 250 Hz or less to capture baseball hitting. Timing of the impact is heavily effected when filtering techniques are being used for data captured at lower sampling rates [69]. Thus, it has been advised to use unfiltered data to calculate bat end velocity in higher sampling rates over 1000 Hz [25]. Therefore, current research was

conducted at 1000 Hz sampling rate, confirming the requirement of high sampling rate to accurately measure coordination of baseball hitting.

Peak angular velocities presented in the previous studies (thorax: $857\text{-}937^{\circ}\text{s}^{-1}$; pelvis: $678\text{-}897^{\circ}\text{s}^{-1}$) are in consistent with the findings of the current study [21, 23, 25]. Small discrepancies could be expected due to the variability of the skill level of the participants and the experimental settings. Explosive movements with high angular velocity in the trunk segments will help players to drive the ball long distance, but improper mechanics may lead to spinal and abdominal muscle injuries. Therefore, regular inspection of the trunk mechanics is important for player performance.

4.5.2. IMU measurement accuracy

Consistency of the measurement is very important. In comparison with gold standard OMCS, IMUs showed high consistency in the Bland-Altman analysis. Even though, OMCS has excellent accuracy, there are practical difficulties in measuring complex movements such as blind spots to detect markers in more than 3 cameras due to marker occlusion and inconsistency when calculating higher order kinematic parameters such as velocity and acceleration. In contrast, IMUs do not have environmental impact on capturing data in complex motions. Also, acceleration and angular velocity data are readily available, which

are useful in calculating joint moment and forces using inverse dynamics techniques [74, 91].

4.5.3. Limitations

Further improvements can be made to the results of this study by minimizing following limitations. First, this study used restricted laboratory settings in order to compare the kinematic measurements with OMCS and thus, baseball hitting was performed in tee-batting conditions instead of live pitching. Sampling rate of 250Hz used in the OMCS was not adequate to accurately measure peak velocities. Precautions were taken to minimize the magnetic distortion for orientation estimation in IMUs, however the error magnitude caused by the ferromagnetic disturbance was not quantified. Some markers were occluded after bat ball impact and thus swing period beyond impact could not be analyzed. However, peak velocities occurred before the impact which showed high accuracy and reliability and therefore, I believe that validity of the data after IMUs does not change significantly.

4.5.4. Summary

This study showed that IMUs attached on thorax, pelvis and hand could accurately detect kinematics during baseball hitting. Baseball hitting is a highly dynamic motion in which parameters change within milliseconds intervals. Therefore, 1000 Hz or higher sampling rate is necessary to accurately measure the coordination of hitting mechanics.

Chapter 5

5. Detection of the ball impact in pitched hitting condition using a hand worn inertial measurement unit

5.1. Introduction

Evaluation of sports specific movements is important to improve player performance. Recently, IMUs have shown tremendous improvement in assessing movements in real game environment which is a challenging task with the use of OMCS. Use of IMUs in individual sports, team sports and water sports has shown the capability of catering different purpose of measurements [92]. Studies have shown that IMU data can be used to measure propulsive movements in wheelchair court sports [93]. Machine learning techniques have been used to analyze IMU data for movement classification in variety of sports [94-96]. Several studies have used IMUs to quantify and classify baseball pitching mechanics [97-99].

Two studies described so far have shown that IMUs can be used to detect important events and have high accuracy and reliability to quantify the kinematics of trunk and hand. However, those studies were limited to tee-bat settings, and thus require validating the system proposed by the two studies in a real baseball field.

Bat speed and ball-exit velocity after hitting are considered primary indices to evaluate hitting performance. Both indices occur at the bat ball impact and thus close detection of bat ball impact timing is very important. Our previous study proposed a method to detect impact using an IMU with 200 Hz sampling rate under tee bat settings with an error of 9 msec. Ball is in contact with the bat less than 1.5 msec at the impact [100]. Thus, high sampling rate about 1000 Hz is essential to detect impact event accurately [25, 101]. This study was performed to understand the error magnitude of the trunk and hand kinematics when the impact time is deviated from its original value. A new algorithm was proposed to accurately detect impact time using a hand worn IMU at 1000 Hz sampling rate. Performance of the aluminum and wooden bats are significantly different [102]. Therefore, both bat types were included in this study.

5.2. Methodology

5.2.1. Participants

Five baseball players (four right-handed and one left-handed; mean age, 20.0 (\pm 0.7) years, mean height, 1.7 (\pm 0.1) m, mean body mass, 72.4 (\pm 10.0) kg) who were the members of University of Miyazaki baseball team participated in this study. The study protocol was approved by the university ethics committee, and written informed consent was obtained

prior to data collection. None of the participants had a known history of musculoskeletal injuries.

5.2.2. Instrumental setup

Three IMUs (sampling rate of 1000 Hz, SS-MS-HMA200G60 (accelerometer ($\pm 1962 \text{ ms}^{-2}$), gyroscope ($\pm 6000 \text{ s}^{-1}$), magnetometer ($\pm 10 \text{ gauss}$)), size: 36 mm (width) \times 53 mm (length) \times 11 mm (depth), weight: 32 g; Sports Sensing Co., Ltd., Fukuoka, Japan) were attached to body segments of the players prior to data collection. One IMU was attached to the superior part of the sternum, and a second IMU was attached between the left and right iliac spines by using a 3D-printed attachment and elasticized tapes (Figure 22). Both IMUs were attached such that the x-axis was parallel to the medio-lateral direction toward the left side, and the y-axis was directed upwards along the longitudinal axis according to anatomical landmarks of the corresponding segments. The third IMU was attached to the dorsal side of the knob-side hand by using double-sided tape over the batting glove and further secured with an elasticized bandage. The positive y-axis of the local coordinates was aligned with the long axis toward the proximal direction, and the z-axis was directed outwards toward the hand. Data captured by each IMU were stored inside the internal memory. Fully charged IMUs were kept on for 10 minutes and accelerometer and magnetometer were then calibrated prior to data collection (Appendix B).



Figure 22: positioning of inertial measurement units (IMUs) on body segments

5.2.3. Data collection during in-field hitting

Baseball field in University of Miyazaki was facilitated to data collection. Each player hit 5 baseballs in two sessions; tee-batting and pitched batting. A pitching machine was used to throw pitches from the pitching mound. Speed was set to regular practice speed. Ball height was adjusted approximately to the waist height when the player is in his stance phase. In each session, players used aluminum and wooden bats to hit baseballs. During the pitched batting session, player hit baseball until 5 successful hits towards the center field. Japanese university players generally use wooden bats in the games. Therefore, each player hit baseballs with their personal wooden bat, but same aluminum bat was used by all the participants throughout the study. Miss hits (ball does not contact with the bat) were

excluded in the analysis. Foul balls, fly balls ground balls and line-drive hits were mapped if further analysis was required (Figure 23).

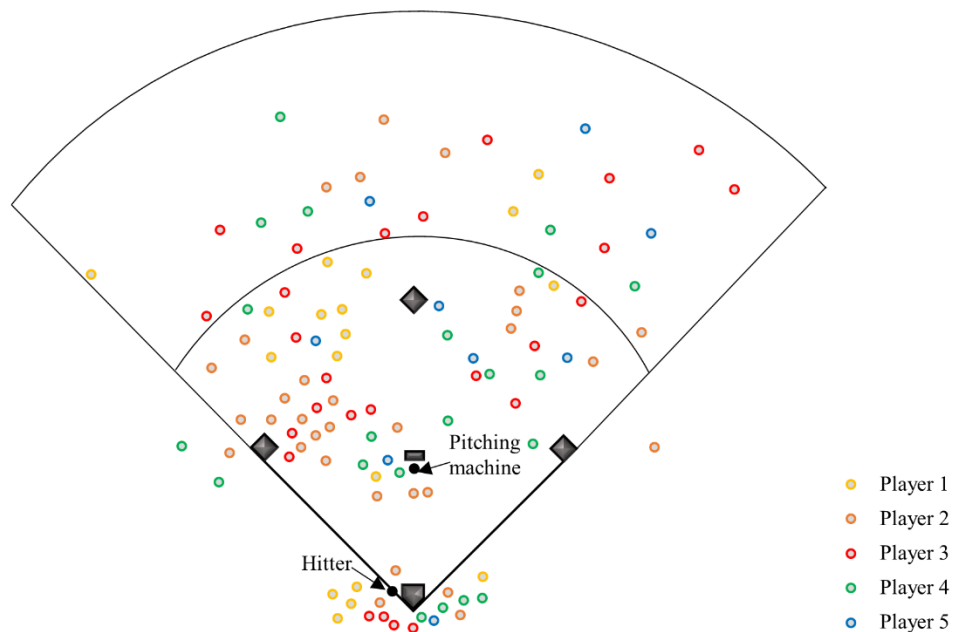


Figure 23: Hit map for pitched balls observed by visual inspection

Before each measurement, players were instructed to stand still for 5 seconds facing home plate and maintaining their sagittal plane parallel to a line drawn from pitching mound to home plate. This allowed to calculate gyroscope bias and initial orientation, which subsequently used as the global coordinate system (pelvis IMU). All the data were transferred to a computer upon data collection. Data were processed offline using a script written in MATLAB (version 2017b, MathWorks®, Natick, MA, USA). Trunk and hand kinematics were calculated as described in the previous chapter.

5.2.4. Impact detection using microphone

A microphone (Module KY-037) placed on the home plate was used to detect the impact time by retrieving the sound signal. Microphone was powered by 5V DC battery and connected to a data acquisition system (DAQ; NR 600, Keyence Cooperation, Osaka, Japan). The DAQ was switched on for 30 minutes to warmup and necessary calibration was followed by before data collection. DAQ was connected to a computer via a USB cable and microphone signal was recorded at 10 kHz sampling rate and stored in the computer in each trial. A 5V pulse trigger was used to synchronize IMU and DAQ.

Microphone signal was stored as a voltage difference. Initial offset was subtracted, and signal was rectified (Figure 24). Initiation of the voltage spike was detected as impact time. Time lag due to the distance between impact location and microphone was calculated by waist height and sound velocity (343 ms^{-1}).

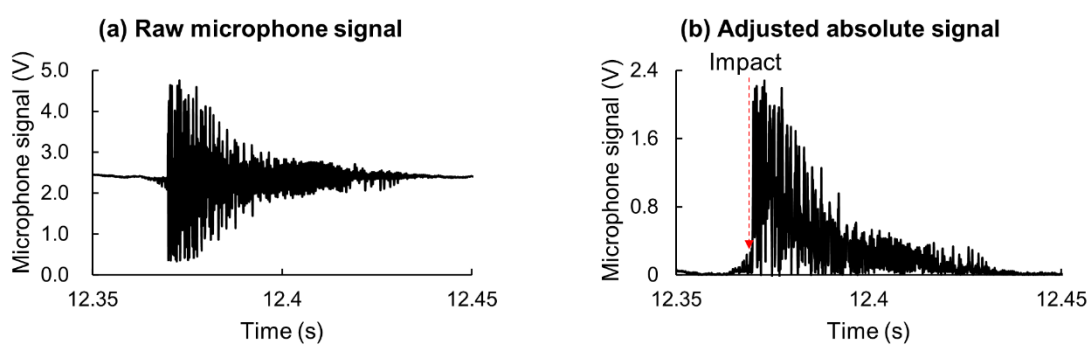


Figure 24: microphone signal at bat-ball impact (a) before and (b) after signal rectification

5.2.5. Impact detection algorithm

Accelerometer data of the IMU attached on the hand was used to derive a new algorithm to detect impact time. Impact time detect by the algorithm was compared with the time retrieved by a microphone. Initial data were collected by swinging a baseball bat freely without hitting a baseball (dry swing) followed by hitting a baseball over a tee pole. Power spectral density of the resultant acceleration in the time domain was observed to understand frequency difference between two signals.

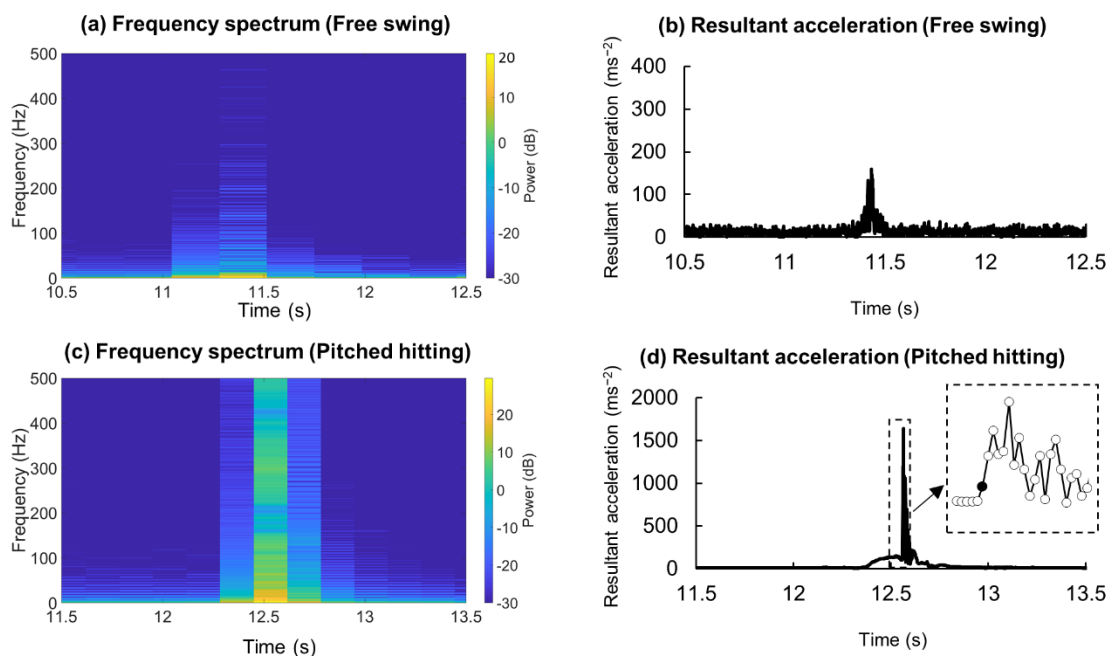


Figure 25: Frequency spectrum of the hand acceleration (a) in free swing and (c) pitched hitting are on left. Corresponding resultant acceleration of the (b) free swing and (d) pitched hitting are on right

It could be observed that general hitting motion of the hand lied under low frequency spectrum (<25 Hz) (Figure 25). However, when ball was collided with the bat, high

frequency power increased suddenly (>100 Hz). This observation was aligned with previous studies that have experimented the dynamics of the bat at bat-ball impact [67, 103].

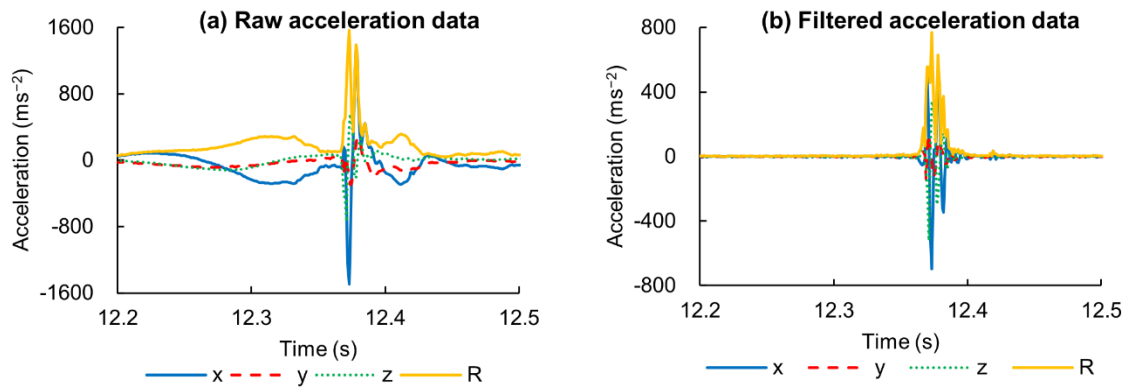


Figure 26: Hand acceleration data (a) before and (b) after using high pass filter

Vibration energy induced at the bat-ball impact is induced and heavily damped at the hands [68]. During baseball swing, IMU attached on the hand recorded the hand acceleration (due to swing motion) and gravity which falls under low frequency range, while the vibration induced on the hand in high frequency range was also recorded. Vibration in the form of acceleration in each axis and corresponding resultant acceleration were further examined. Accelerometer data were high pass filtered using a zero-lag fourth order Butterworth filter with cut off frequency of 100 Hz to isolate the vibration signal (Figure 26). When the filtered resultant acceleration signal was closely examined, it could be noticed that neither maximum value, nor a local peak were coincided with the exact impact location retrieved by the microphone (Figure 27).

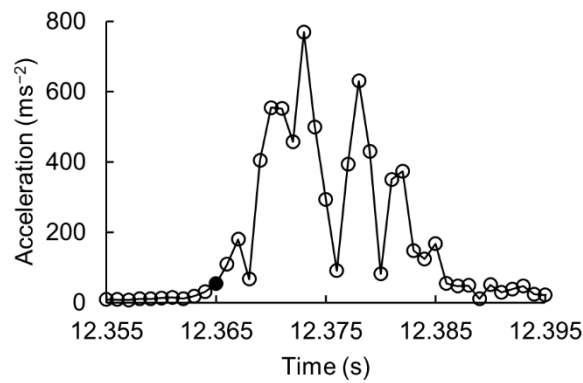


Figure 27: Filtered resultant acceleration profile. Impact time detected by the microphone is denoted with black dot

Therefore, filtered acceleration data in each local axis (x , y , z) were further examined. Feel of the vibration on the hands depend on the bat-ball contact angle, point of impact and the grip strength. Variation of the amplitude in each local axis in different hitting output (Figure 28; (a) Line drive, (b) foul ball, (c) ground ball, (d) fly ball) could be observed. However,

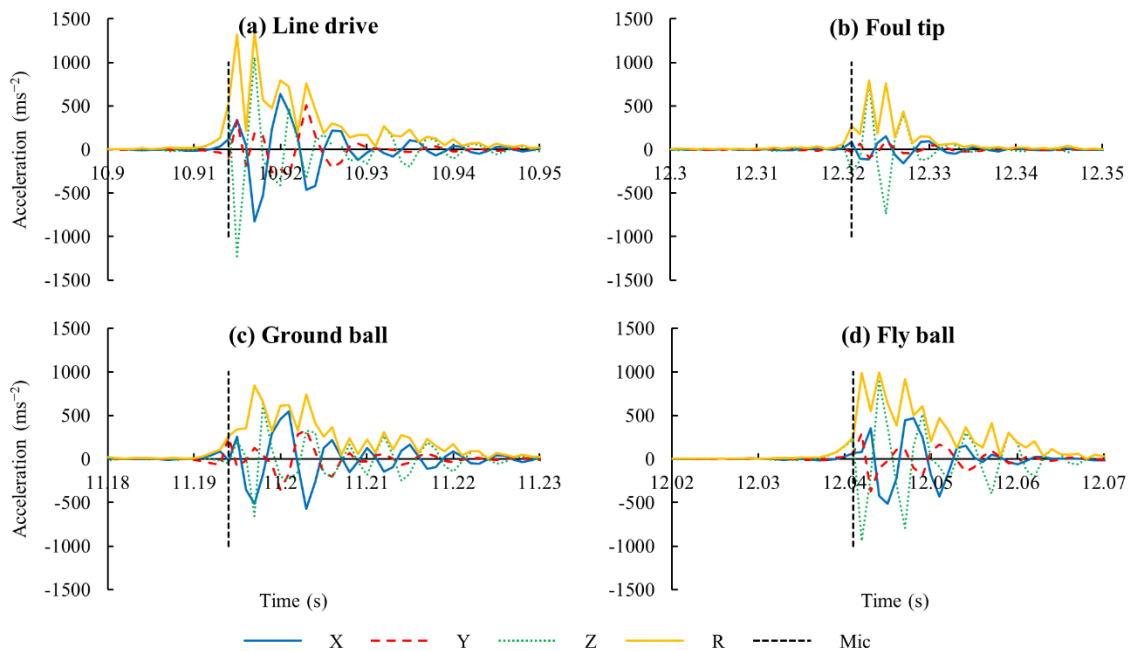


Figure 28: Filtered acceleration of the hand IMU (x , y , z local axes and corresponding resultant acceleration R) in different hitting outcomes. (a) Line drive, (b) Foul tip, (c) Ground ball, (d) Fly ball

peak value of the x, y, z axes were not coincided with the impact time retrieved from the microphone, but initial local peak in one of the local axes was coincided. The axis coincided with the impact time varied with different impact outcomes and thus specific axis could not be chosen. It could be noticed that acceleration amplitude of the filtered data was very different depending on the outcome of the batted ball and thus a common threshold value over which the first local peak was not easily determined. Thus, absolute difference of the acceleration of each axis was used, and the earliest local maximum was set to detect the impact time (Figure 29). Complete algorithm is described in the flow chart (Figure 30).

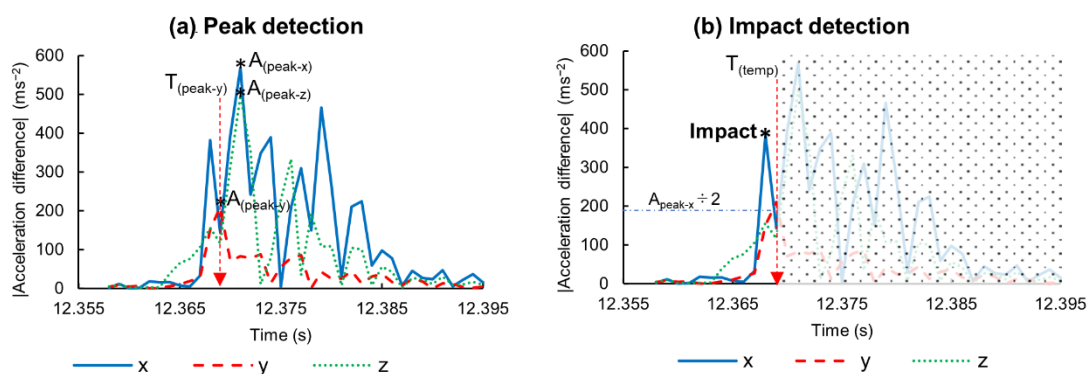


Figure 29: Detection of local peaks in each axis of the hand acceleration and impact time detection

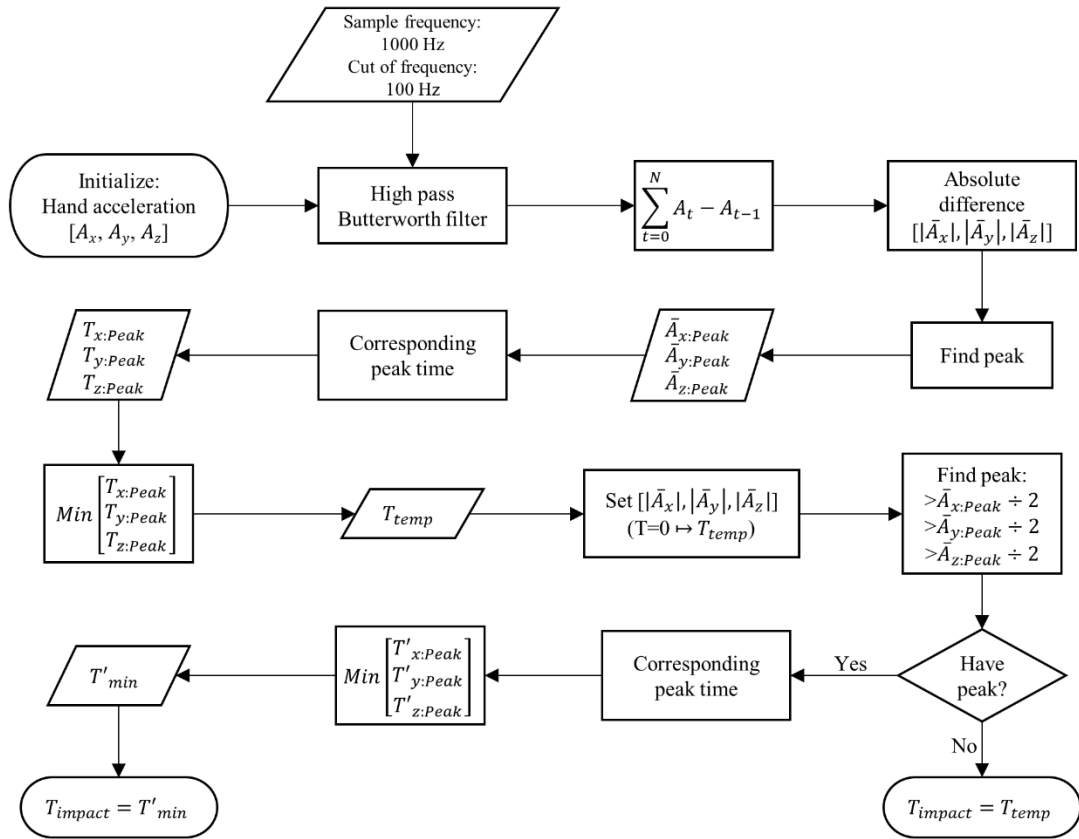


Figure 30: Impact algorithm flow chart

5.3. Statistical analysis

A trial was considered successful if the bat contacted with ball and an audible bat-ball contact was heard. Altogether, 157 trials (68 trials from Aluminum bat(Tee = 25, pitched = 43), 89 trials from wooden bats (Tee = 25, pitched = 64)) were taken for the analysis. Figure 31 shows the breakdown of the outcome of the hitting experiment.

Deviation of the trunk and hand kinematics from their corresponding impact time (retrieved from microphone) were calculated for ± 10 msec. Only tee-batting trials were considered to reduce inter-player variation. Mean deviation of the segmental angles, angular velocities, linear velocities, and linear accelerations were taken for the evaluation. Deviation was represented in mean absolute error (MAE) as a percentage of the corresponding peak value. MAE $< 5\%$ was considered excellent agreement and $< 10\%$ considered acceptable.

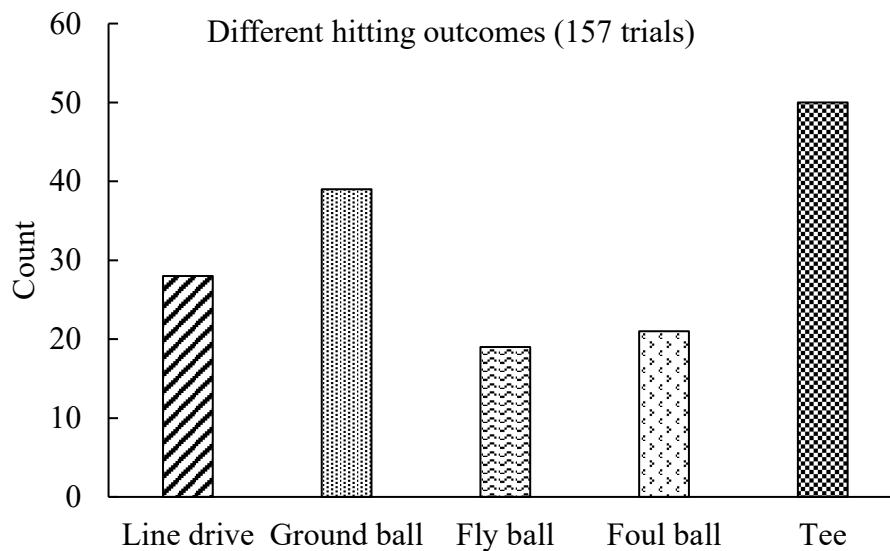


Figure 31: Overall hit count in different hitting outcomes

To evaluate the validity of new algorithm, mean time difference, standard deviation (SD) and root mean square error (RMSE) was calculated. Levene's test was used to confirm the homogeneity of variance between hitting sessions (tee vs. pitched) for each bat type (aluminum vs. wooden). Two-way analysis of variance (ANOVA) was used to evaluate estimate significant difference between bat-types or hitting types to detect the impact time

using new algorithm. Level of significance vs set to 0.05. Data analysis was completed using statistical package for social sciences (SPSS; version 22.0, IBM Corp., Tokyo, Japan).

5.4. Results

5.4.1. Deviation of the kinematics values from impact

Deviation of the angular velocity, linear velocity, and linear acceleration from impact as a percentage of corresponding peak value were calculated. Segmental angular velocities in the vertical axis (Y-axis), linear velocity, and acceleration toward the pitcher's direction (X-axis) are plotted in Figure 32 (a–c) and corresponding MAE are plotted in Figure 32 (d–f) respectively. Peak angular velocity of the hand was at impact, and thus when deviation represented as percentage of peak, it was close to zero. Both angular velocity and linear velocity errors reached $\geq 10\%$ beyond ± 7 msec in one segment at least, whereas the error was $< 5\%$ within ± 3 msec. Linear acceleration error exceeded 10% beyond ± 4 msec, which required the impact time to be detected within ± 2 msec to reduce the error to $< 5\%$. The MAEs of the thorax and pelvis angles were $\leq 10\%$ within ± 10 msec and so are not included in the figures.

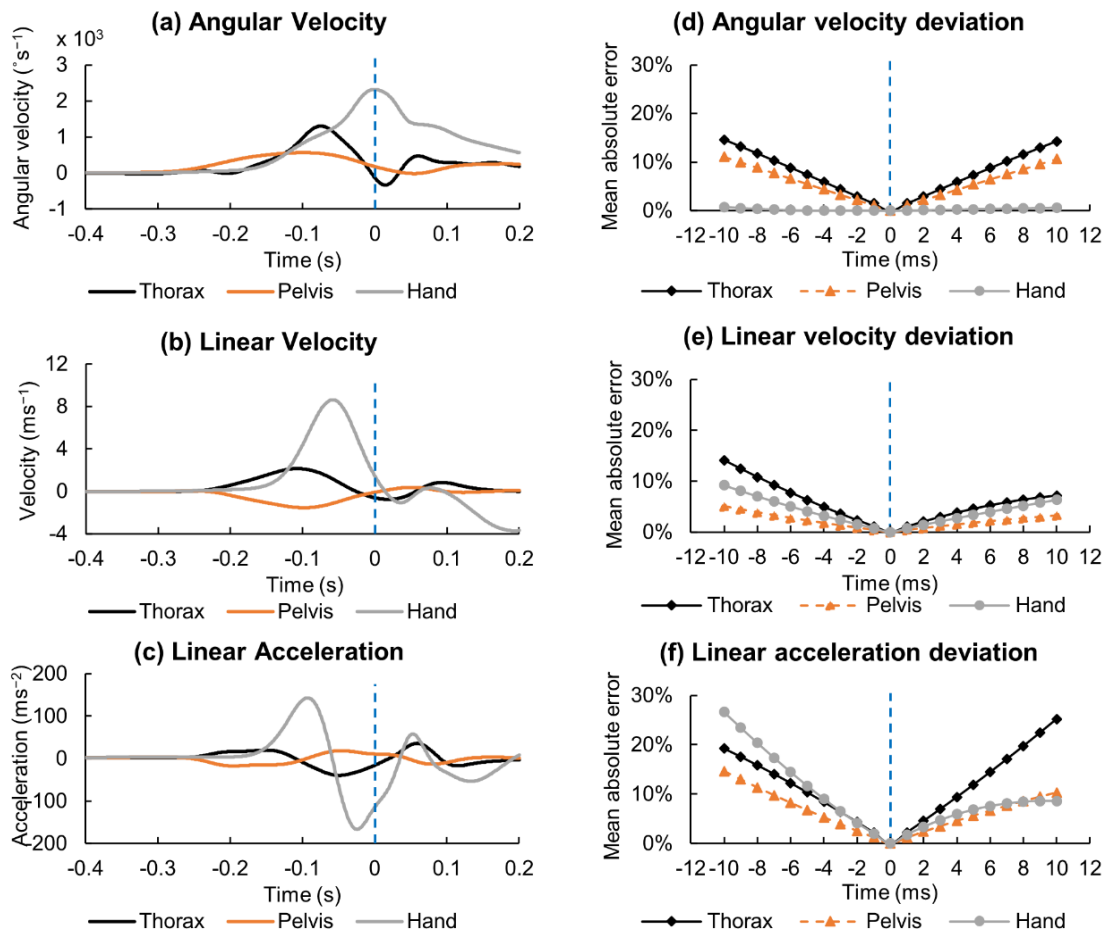


Figure 32: Kinematic profiles and corresponding deviation calculated as mean absolute error

5.4.2. Impact time error

The time difference detected by the hand IMU and the microphone at the bat–ball impact was assessed separately for aluminum and wooden bats in each session and presented as the mean error, SD, and RMSE in Table 5.

Table 5: Mean error, standard deviation and root mean square error of the impact time detected by new algorithm using hand acceleration

Bat Type	Hitting Session	Mean (SD)	RMSE
Aluminum	Pitched	1.1 (± 0.8)	1.3
	Tee	1.2 (± 0.6)	1.4
	All	1.1 (± 0.7)	1.3
Wood	Pitched	1.2 (± 0.8)	1.4
	Tee	1.3 (± 1.0)	1.6
	All	1.2 (± 0.9)	1.5

Mean error and RMSE were consistent at 1 msec, with SD of 0.9 msec or less in each bat type. Levene statistics confirmed the equality of variances among hitting sessions for the aluminum bat ($F = 0.202$, $p = 0.65$) and for wooden bat ($F = 1.489$, $p = 0.226$). There were no statistically significant differences in the mean error between bat types ($p = 0.466$) and hitting sessions ($p = 0.300$).

5.5. Discussion

Baseball hitting is a highly dynamic activity where biomechanical parameters change within millisecond time intervals. During the swing phase, rotational torque of the bat is increasing followed by translation power just before the ball impact to increase BEV [104]. These

measurements need to be acquired accurately to understand performance parameters. Thus, it is important to break down the biomechanical description of baseball hitting in a timely manner. The study results revealed that the selected kinematic parameters varied as much as 20% when the timing of the bat–ball impact deviated ± 10 msec from the actual timing. Therefore, requirement of detecting the impact timing within ± 2 msec was revealed. Method proposed in this study detected the impact time within 1 msec of error, indicating excellent accuracy for identifying bat–ball impact by using a hand-worn IMU.

5.5.1. Accuracy of bat–ball impact timing

Orientation angles of the trunk segments did not show significant variation ($MAE < 10\%$) when impact time is deviated ± 10 msec. However, impact time should be captured within ± 7 msec for linear and angular velocity variables to be acceptable ($MAE < 10\%$) and ± 3 msec was expected to accurately measure ($MAE < 5\%$) the kinematics. Linear acceleration further limited the accuracy to ± 2 msec for excellent agreement. Therefore, high-speed cameras and OMCS require capturing biomechanical parameters at 500 Hz or higher sampling rate to accurately monitor higher-order derivatives at bat–ball impact.

Impact error is slightly less in pitched hitting than in stationary baseball hitting (Figure 29).

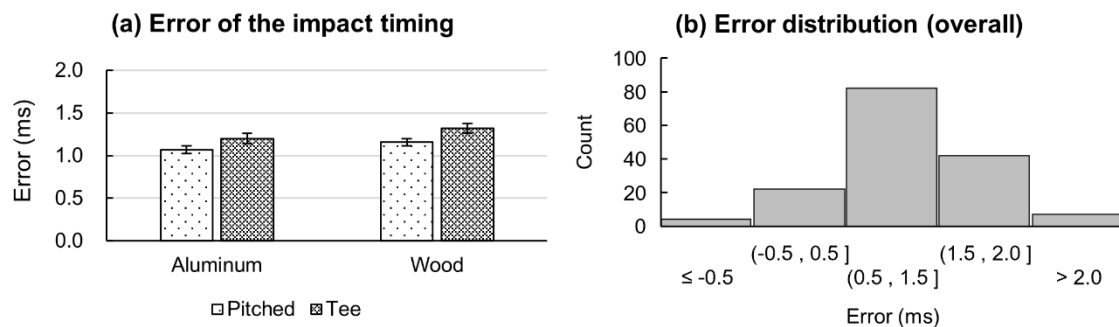


Figure 33: (a) Impact error in aluminum and wooden bat in each tee and pitched bat session, (b) overall error distribution graph

Baseball bat is in contact with the ball for a shorter period during high-speed collisions (pitched) than during low-speed collisions (tee) [103]. Energy is dispersed through the bat faster in the form of vibration and thus, the propagated signal could be detected at the end of the bat quicker for shorter collision times than for longer collision times. Additionally, peak reaction force occurs earlier in aluminum bats than in wooden bats when the bat collides with a baseball [105]. However, the time difference between groups was less than 1 msec, which is the smallest reliable measurement when sampling at 1000 Hz. Therefore, no significant difference could be measured between the bat types or hitting sessions.

The errors of the impact timing detected by a hand IMU showed an approximately normal distribution centered at 1 msec (Figure 33 (b)). The overall error distribution demonstrated that the method introduced in this study had minimal systematic errors for detecting bat–ball impact [106].

5.5.2. Hand acceleration caused by impact force

There are many factors concerning the vibration of the bat after bat-ball collision. They are, coefficient of restitution of bat and ball (which is a function of material), impact location of the bat, contact angle, ball and bat velocity at the impact. Vibration magnitude exerted on the hand vary with grip firmness and impact location [67]. Acceleration of each axis showed different amplitudes in each trial depending on the impact location and contact angle (Figure 34). The first peak was not necessarily the highest peak on each axis due to different frequency modes, and therefore, required a second iteration to closely detect the impact time. Furthermore, the acceleration magnitude was not consistent for each bat-ball contact. Therefore, a common threshold value could not be determined to detect the first local peak. Thus, the acceleration difference was calculated, and half of the highest peak was used as the threshold value to determine the impact time. The dynamics of the baseball swing could be calculated if the IMU was fixed on the bat knob [101]. However, impact vibration exceeded the accelerometer measurement range (1962 ms^{-2}) during the initial testing, which could damage the accelerometer. Further, some players felt discomfort when gripping the bat near the knob, so the IMU was attached to the dorsal side of the hand.

Theoretically, when a ball contacts on a bat, the frequency spectrum due to the impact range from 0 to $1/\tau$ where τ is the duration of impact [68]. When impact duration is practically examined, it is calculated to be 1.5 msec, which lead to the frequency spectrum ranges up

to 667 Hz [67]. An IMU with 1000 Hz sampling rate could only detect frequency up to 500 Hz according to Nyquist frequency. Thus, higher sampling rates could observe the impact time better. Anyway, our results showed that the impact time should be detected within 2 msec of maximum error for accurate kinematic measurements. Therefore, 1000 Hz IMU was good enough to detect impact time in the context of accurate kinematic measurements.

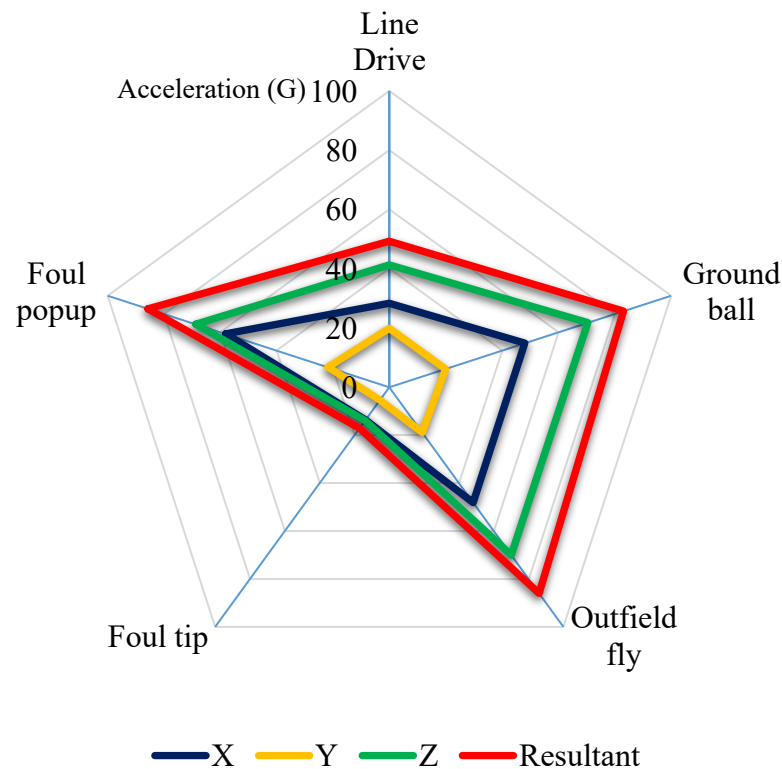


Figure 34: Mean acceleration peaks in different outcomes after bat-ball impact

5.5.3. Limitations

Only trunk and hand kinematics were calculated to assess the variability at the bat-ball impact. Hitting motion starts at the lower extremities, and coordination of the motion is gradually transferred to the upper extremities during bat-ball impact during the swing phase.

Thus, trunk and hand kinematics are well-selected parameters for evaluation. However, the variation of the bat head speed around the impact time should be further evaluated. It was assumed that the ball was hit directly over the microphone at waist height, but the spatial margin of error may have affected detection of the impact time in the pitched ball hitting sessions. Nevertheless, the impact detected by the algorithm had an error range between -1 msec and 3 msec.

5.5.4. Summary

This study showed that bat–ball impact time should be detected within ± 2 ms to accurately monitor higher-order trunk and hand kinematics in baseball hitting. Therefore, the results of the study suggest using high sampling rates for baseball-hitting analysis when using an OMCS or high-speed cameras. IMUs have recently shown promising accuracy for baseball-hitting analysis. A new algorithm was introduced using a hand-worn IMU at 1000 Hz sampling rate to accurately detect bat–ball impact time within 2 msec of error.

Chapter 6

6. Conclusion and future recommendations

6.1. Conclusion

Evidence-based scientific approaches are becoming popular in any sport to educate players for better performance while reducing injuries. Baseball is one such a sport involves advanced technologies to detect players body movements. Baseball hitting is playing a key role in the game. Hitting motion have been evolved from the inception of the game, but still it is considered one of the most difficult activities in any sport as it requires the edge of human limitations to hit a ball thrown at 150 kmh^{-1} .

Baseball hitting motion have been analyzing since mid-1960s. Video cameras had been used initially, until three-dimensional motion capture technology was introduced. Since then, high speed motion capture data were recorded and biomechanical description of baseball hitting has been reported. Sports scientists have divided baseball hitting motion into four major phases detected by three key events for comprehensive analyses. Usually, these events are detected using cameras and force plates. However, camera-based motion capture systems require fixed space and thus hitting analyses were limited inside laboratories. This has further restricted the analyses by hitting a stationary ball over live pitching. Therefore,

alternative motion capture system is necessary to record and analyze hitting motion in game settings.

Inertial measurement units (IMUs) have shown promising results in gait analysis and different sporting applications. This study was aimed to detect important hitting events and validation of selected kinematics in baseball hitting using IMUs. Baseball hitting requires both lower body and upper body to generate translational and rotational power to hit a baseball. To understand thoroughly, hitting sequence is generally described in four different phases identified by foot-off, foot-on and bat-ball impact events.

First experiment of this study showed that acceleration data of the IMUs attached on pelvis and hand could detect the key events under tee-batting conditions. Hitting motion is linear towards the pitcher's direction until foot on event. Propulsive and breaking forces during foot-off and foot on events had a significant acceleration difference on the trunk. Thus, IMU attached on pelvis could detect foot events. This study was restricted to tee bat settings and thus impact detection was further validated in pitched hitting in a subsequent experiment.

Trunk motion in baseball hitting has shown significant importance to increase bat velocity and modulate coordination to hit different pitch types. Thus, accuracy and reliability of the trunk and hand kinematics were evaluated. Results showed that pelvis, thorax segmental angles together with spine angles were measured with excellent accuracy (RMSE < 5°).

Further, angular velocities and hand velocities also showed excellent to good accuracy (MAE < 10%). IMUs proved to be accurate in measuring trunk and hand kinematics when compared with gold standard optical motion capture system.

Further, impact time detection was validated in real game settings. It was shown that many kinematic parameters change significantly at bat-ball impact event and require the impact event to be detected with 2 msec margin of error. A new algorithm was developed to accurately detect bat-ball impact using an IMU attached on the hand. Further, importance of higher sampling rate was also described and suggested that at least 500 Hz or higher sampling rate is necessary to accurately monitor kinematics and coordination of hitting.

6.2. Future recommendations

Hitting kinematics have shown significant differences for tee-batting when compared live pitching using a pitching machine. However, due to technological constraints, none of the studies have performed in a real baseball field at high sampling rate to accurately measure hitting kinematics. Proposed method in this study is feasible to understand kinematic differences between training methods (tee-batting, toss batting) with live pitching (thrown by a pitcher). Further, differences in vibration energy dispersed on the hand could be observed in different hitting outcomes (line drive, foul tip etc.,). Linear and angular momentum of the bat at ball impact is a good performance indicator. How much power is

transferred on the ball may have a relationship with the vibration exerted on the hand. This should be further studied. Setting up the IMU system is fast and easy. Therefore, regular training can be recorded in daily basis. Data collected regularly can be used with machine learning algorithms to further evaluate intra-player and inter-player variations as training progress. An updated database is useful in recognizing performance patterns to improve training methods and hitting motion.

Appendix A

Construction of the rotation matrix

Orientation of a rigid body in Euclidean space can be represented by a proper orthogonal matrix, known as rotation matrix [107]. Let the angles of 3 successive rotations of X, Y and Z axes be α , β and γ . Rotation matrix of each axis can be written as follows.

$$R(x) = \begin{pmatrix} 1 & 0 & 0 \\ 0 & \cos \alpha & -\sin \alpha \\ 0 & \sin \alpha & \cos \alpha \end{pmatrix}$$

$$R(y) = \begin{pmatrix} \cos \beta & 0 & \sin \beta \\ 0 & 1 & 0 \\ -\sin \beta & 0 & \cos \beta \end{pmatrix}$$

$$R(z) = \begin{pmatrix} \cos \gamma & -\sin \gamma & 0 \\ \sin \gamma & \cos \gamma & 0 \\ 0 & 0 & 1 \end{pmatrix}$$

Orientation matrix R be then calculated by the multiplication of the three rotations.

$$R = R(z)R(y)R(x)$$

$$R = \begin{pmatrix} \cos \gamma & -\sin \gamma & 0 \\ \sin \gamma & \cos \gamma & 0 \\ 0 & 0 & 1 \end{pmatrix} \begin{pmatrix} \cos \beta & 0 & \sin \beta \\ 0 & 1 & 0 \\ -\sin \beta & 0 & \cos \beta \end{pmatrix} \begin{pmatrix} 1 & 0 & 0 \\ 0 & \cos \alpha & -\sin \alpha \\ 0 & \sin \alpha & \cos \alpha \end{pmatrix}$$

$$R = \begin{pmatrix} \cos \beta \cos \gamma & -\cos \alpha \sin \gamma + \sin \alpha \sin \beta \cos \gamma & \sin \alpha \sin \gamma + \cos \alpha \sin \beta \cos \gamma \\ \cos \beta \sin \gamma & -\cos \alpha \cos \gamma + \sin \alpha \sin \beta \sin \gamma & -\sin \alpha \cos \gamma + \cos \alpha \sin \beta \sin \gamma \\ -\sin \gamma & \sin \alpha \cos \beta & \cos \alpha \cos \beta \end{pmatrix}$$

The rotation matrix can then be used to transform the vector on local coordinates to the global coordinates. If the acceleration vector in the local coordinates is $[a_x, a_y, a_z]$, the corresponding global vector $[A_x, A_y, A_z]$ can be calculated as,

$$\begin{bmatrix} A_x \\ A_y \\ A_z \end{bmatrix} = \begin{pmatrix} \cos \beta \cos \gamma & -\cos \alpha \sin \gamma + \sin \alpha \sin \beta \cos \gamma & \sin \alpha \sin \gamma + \cos \alpha \sin \beta \cos \gamma \\ \cos \beta \sin \gamma & -\cos \alpha \cos \gamma + \sin \alpha \sin \beta \sin \gamma & -\sin \alpha \cos \gamma + \cos \alpha \sin \beta \sin \gamma \\ -\sin \gamma & \sin \alpha \cos \beta & \cos \alpha \cos \beta \end{pmatrix} \begin{bmatrix} a_x \\ a_y \\ a_z \end{bmatrix}$$

Appendix B

Sensor calibration

Accelerometer calibration

Accelerometer and the outer plastic box could have misalignment and thus require calibration. IMUs were stacked in a 3D printed cubical box. All the IMUs were stacked in the same orientation. Box was placed on a flat surface and static acceleration data were recorded in 6 different orientations to measure gravity from each axis ($X+$, $X-$, $Y+$, $Y-$, $Z+$, $Z-$).

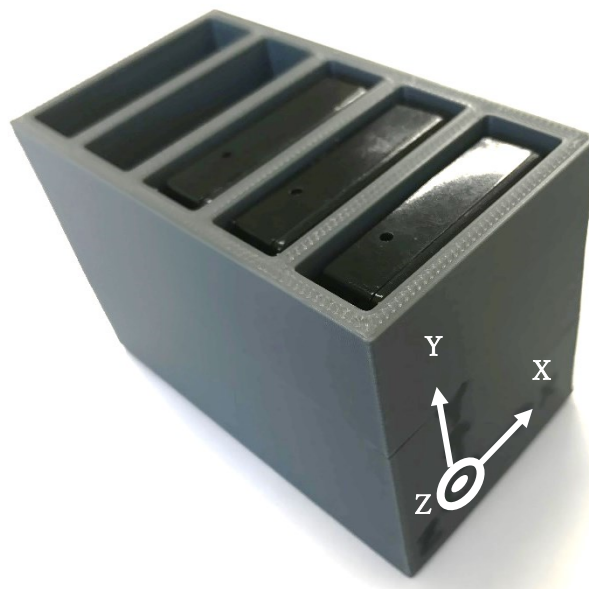


Figure 35: calibration box of the inertial measurement units

If perfectly aligned with the axis of gravity, vertical axis should show the value of $\pm 1G$ ($G = 9.81 \text{ ms}^{-2}$) depending on the direction of the axis while other axes have an acceleration of zero. An example of the mean values in each axis for 5 s period is given below.

Table 6: Calibration data of the accelerometer

True Value (G)	X (G)	Y (G)	Z (G)
-1	-1.032	-1.054	-0.949
0	-0.039	-0.046	0.001
1	0.978	0.952	0.975

Bias and gain were then calculated by plotting the values for each axis and calculating the intercept and coefficient.

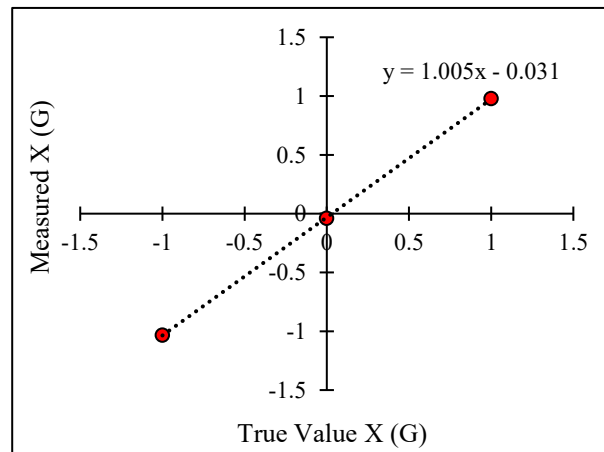


Figure 36: Regression graph of the measured and true values during accelerometer calibration

As per above graph, gain for x-axis is 1.005 and the bias is -0.031 . Calibrated acceleration data can then be calculated by the following equation.

$$\text{Calibrated value} = (\text{Measured value} - \text{bias}) \div \text{gain}$$

Magnetometer calibration

Magnetometer measurements are sensitive to soft and hard iron distortions as described in chapter 2. Motion analysis laboratories are equipped with computers and metal construction materials that can interfere the magnetometer data [108]. Therefore, proper calibration prior to data collection was required to accurately measure IMU orientation.

IMUs were stacked inside the cubic box and magnetometer data were recorded for 30 s by randomly rotated in each axis inside data capture volume. Distorted magnetometer data were then compared with the norm of the earth's magnetic field using Magneto 1.2 software. This software has adopted the ellipsoid fitting technique to calculate the scale factors matrix (A) and the bias (b) [109]. Norm of the magnetic field is different in each location. World magnetic model was used to calculate the actual magnetic field from the latitude (31.84062 North) and longitude (131.39771 East) reference of the rehabilitation center [110].

Calibrated magnetometer data from the trials were then calculated using the calibration parameters using the following equation.

$$\textit{Calibrated data} = A^{-1} \times (\textit{Distorted data} - b)$$

Magnetometer rotated in a 3D space in a distortion free environment have the origin of the vector at $(0, 0, 0)$ and data can be plotted on a surface of a sphere with radius equivalent to the norm of the earth's magnetic field. However, soft and hard iron distortion will shift the origin and change the sphere into asymmetric shape. Calibration parameters will calculate the origin shift and the parabolic factors to remove the distortion.

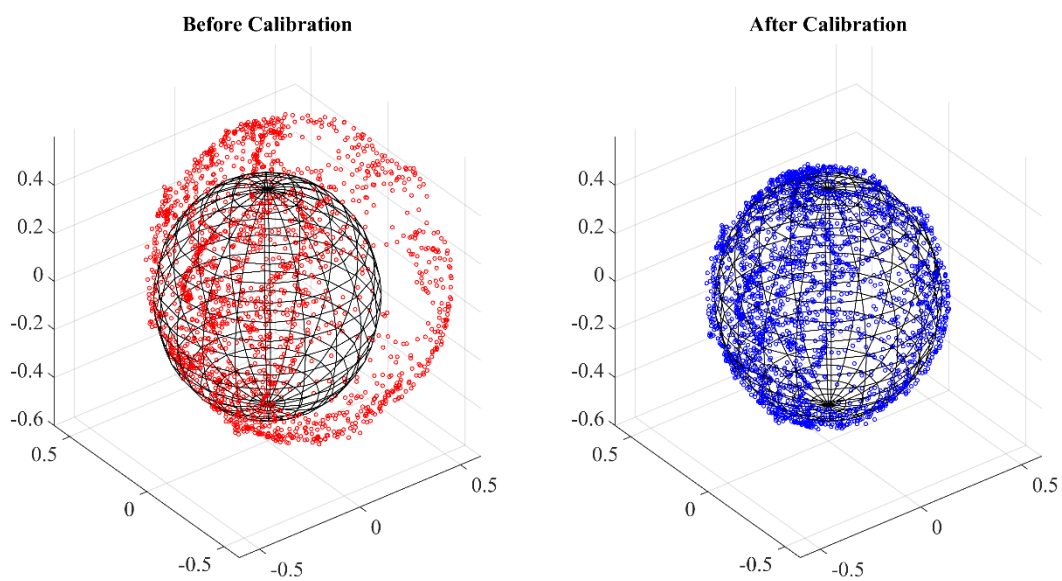


Figure 37: Data plotted in 3D space before and after magnetometer calibration

Appendix C

Quaternions

Quaternion is a 4-tuple or a four-element representation of the orientation in 3D Euclidean space. Quaternion (q) can be written as $q = q_0 + q_1\mathbf{i} + q_2\mathbf{j} + q_3\mathbf{k}$, subjected to $\mathbf{ij} = \mathbf{jk} = \mathbf{ki} = -1$. q_0 is known as scalar part while $q_1\mathbf{i} + q_2\mathbf{j} + q_3\mathbf{k}$ is the vector part. Quaternion in general is written in 4 components $q = [q_0, q_1, q_2, q_3]$.

Some of the quaternion properties are given below.

Complex conjugate

Complex conjugate of the quaternion q is represented as q^* .

If $q = q_0 + q_1\mathbf{i} + q_2\mathbf{j} + q_3\mathbf{k}$, then $q^* = q_0 - q_1\mathbf{i} - q_2\mathbf{j} - q_3\mathbf{k}$.

Quaternion conjugate adheres the following rule.

$$(pq)^* = q^*p^* \text{ and } (p^*q)^* = q^*p$$

Quaternion norm

Quaternion norm is denoted by $N(q)$

$$N(q) = \sqrt{q^*q}$$

Quaternion multiplication

Let two quaternions be $a_1 + b_1\mathbf{i} + c_1\mathbf{j} + d_1\mathbf{k}$ and $a_2 + b_2\mathbf{i} + c_2\mathbf{j} + d_2\mathbf{k}$

Product of the two quaternions (also known as Hamilton product) gives the following expression.

$$\begin{aligned} & a_1a_2 + a_1b_2\mathbf{i} + a_1c_2\mathbf{j} + a_1d_2\mathbf{k} \\ & + b_1a_2\mathbf{i} + b_1b_2\mathbf{i}^2 + b_1c_2\mathbf{ij} + b_1d_2\mathbf{ik} \\ & + c_1a_2\mathbf{j} + c_1b_2\mathbf{ij} + c_1c_2\mathbf{j}^2 + c_1d_2\mathbf{jk} \\ & + d_1a_2\mathbf{k} + d_1b_2\mathbf{ik} + d_1c_2\mathbf{jk} + d_1d_2\mathbf{k}^2 \end{aligned}$$

The product of the two quaternion is equivalent to successive rotation of $a_2 + b_2\mathbf{i} + c_2\mathbf{j} + d_2\mathbf{k}$ followed by $a_1 + b_1\mathbf{i} + c_1\mathbf{j} + d_1\mathbf{k}$.

Quaternion multiplication is denoted by the symbol \otimes

Quaternion to rotation matrix

Quaternion can be converted into 3×3 rotation matrix by following equation.

$$R(q) = \begin{bmatrix} 1 - 2q_2^2 - 2q_3^2 & 2q_1q_2 + 2q_1q_2 & 2q_1q_3 - 2q_0q_2 \\ 2q_1q_2 - 2q_1q_2 & 1 - 2q_1^2 - 2q_3^2 & 2q_2q_3 + 2q_0q_1 \\ 2q_1q_3 + 2q_0q_2 & 2q_2q_3 - 2q_0q_1 & 1 - 2q_1^2 - 2q_2^2 \end{bmatrix}$$

Euler angles can be derived from the rotation matrix in the following form:

YXZ sequence (R_{ij} ; i and j indicate the row and column of the rotation matrix)

$$\text{Rotation around } x \text{ axis} = \tan^{-1} \left(\frac{R_{31}}{R_{33}} \right)$$

$$\text{Rotation around } y \text{ axis} = \tan^{-1} \left(\frac{-R_{23}}{\sqrt{1 - R_{31}^2}} \right)$$

$$\text{Rotation around } z \text{ axis} = \tan^{-1} \left(\frac{R_{21}}{R_{22}} \right)$$

References

1. Williams, T. and J. Underwood, Science of hitting. 1986: *Simon and Schuster*.
2. Adair, R.K., The physics of baseball. 2002: *HarperCollins, New York*.
3. Katsumata, H., A functional modulation for timing a movement: a coordinative structure in baseball hitting. *Hum Mov Sci*, 2007. **26**(1): p. 27-47.
4. Conte, S.A., M.M. Thompson, M.A. Marks, and J.S. Dines, Abdominal Muscle Strains in Professional Baseball:1991-2010. *The American Journal of Sports Medicine*, 2012. **40**(3): p. 650-656.
5. Mlynarek, R.A. and S.H. Coleman, Hip and Groin Injuries in Baseball Players. *Current Reviews in Musculoskeletal Medicine*, 2018. **11**(1): p. 19-25.
6. Breen, J.L., What makes a good hitter? *Journal of Health, Physical Education, Recreation*, 1967. **38**(4): p. 36-39.
7. Messier, S.P. and M.G. Owen, Bat Dynamics of Female Fast Pitch Softball Batters. *Research Quarterly for Exercise and Sport*, 1984. **55**(2): p. 141-145.
8. Race, D.E., A Cinematographic and Mechanical Analysis of the External Movements Involved in Hitting a Baseball Effectively. *Research Quarterly. American Association for Health, Physical Education and Recreation*, 1961. **32**(3): p. 394-404.

9. Messier, S.P. and M.G. Owen, The Mechanics of Batting: Analysis of Ground Reaction Forces and Selected Lower Extremity Kinematics. *Research Quarterly for Exercise and Sport*, 1985. **56**(2): p. 138-143.
10. Shapiro, R. and N.R. Miller, Three-dimensional kinetic analysis of the baseball swing. *Journal of Biomechanics*, 1982. **15**(4): p. 340.
11. Abdel-Aziz, Y., Karara. HM. Direct linear transformation from comparator coordinates into object-space coordinates in close-range photogrammetry. in *ASP Symposium on Close Range Photogrammetry*. 1971.
12. Shapiro, R., Direct Linear Transformation Method for Three-Dimensional Cinematography. *Research Quarterly. American Alliance for Health, Physical Education and Recreation*, 1978. **49**(2): p. 197-205.
13. Ceseracciu, E., Z. Sawacha, and C. Cobelli, Comparison of markerless and marker-based motion capture technologies through simultaneous data collection during gait: proof of concept. *PloS one*, 2014. **9**(3): p. e87640.
14. Kim, S. and M.A. Nussbaum, Performance evaluation of a wearable inertial motion capture system for capturing physical exposures during manual material handling tasks. *Ergonomics*, 2013. **56**(2): p. 314-326.
15. Metcalf, C.D., R. Robinson, A.J. Malpass, T.P. Bogle, T.A. Dell, C. Harris, and S.H. Demain, Markerless motion capture and measurement of hand kinematics:

- validation and application to home-based upper limb rehabilitation. *IEEE Transactions on Biomedical Engineering*, 2013. **60**(8): p. 2184-2192.
16. Mündermann, L., S. Corazza, and T.P. Andriacchi, The evolution of methods for the capture of human movement leading to markerless motion capture for biomechanical applications. *Journal of neuroengineering and rehabilitation*, 2006. **3**(1): p. 1-11.
 17. Nakata, H., A. Miura, M. Yoshie, and K. Kudo, Electromyographic activity of lower limbs to stop baseball batting. *The Journal of Strength & Conditioning Research*, 2012. **26**(6): p. 1461-1468.
 18. Shaffer, B., F.W. Jobe, M. Pink, and J. Perry, Baseball batting. An electromyographic study. *Clinical orthopaedics and related research*, 1993(292): p. 285-293.
 19. Brodie, M.A., M.J. Coppens, S.R. Lord, N.H. Lovell, Y.J. Gschwind, S.J. Redmond, M.B. Del Rosario, K. Wang, D.L. Sturnieks, and M. Persiani, Wearable pendant device monitoring using new wavelet-based methods shows daily life and laboratory gaits are different. *Medical & biological engineering & computing*, 2016. **54**(4): p. 663-674.
 20. Reinecke, K., M. Cordes, C. Lerch, F. Koutsandréou, M. Schubert, M. Weiss, and J. Baumeister, From Lab to Field Conditions: A Pilot Study on EEG Methodology in Applied Sports Sciences. *Applied Psychophysiology and Biofeedback*, 2011. **36**(4):

- p. 265-271.
21. Welch, C.M., S.A. Banks, F.F. Cook, and P. Draovitch, Hitting a baseball: A biomechanical description. *Journal of orthopaedic & sports physical therapy*, 1995. **22**(5): p. 193-201.
 22. Putnam, C.A., Sequential motions of body segments in striking and throwing skills: descriptions and explanations. *Journal of biomechanics*, 1993. **26**: p. 125-135.
 23. Escamilla, R.F., G.S. Fleisig, C. DeRenne, M.K. Taylor, C.T. Moorman, R. Imamura, E. Barakatt, and J.R. Andrews, A Comparison of Age Level on Baseball Hitting Kinematics. *Journal of Applied Biomechanics*, 2009. **25**(3): p. 210-218.
 24. Inkster, B., A. Murphy, R. Bower, and M. Watsford, Differences in the kinematics of the baseball swing between hitters of varying skill. *Journal of Science and Medicine in Sport*, 2010. **12**: p. e12-e13.
 25. Dowling, B. and G.S. Fleisig, Kinematic comparison of baseball batting off of a tee among various competition levels. *Sports Biomech*, 2016. **15**(3): p. 255-69.
 26. Ranganathan, R. and L.G. Carlton, Perception-action coupling and anticipatory performance in baseball batting. *Journal of motor behavior*, 2007. **39**(5): p. 369-380.
 27. Ae, K., S. Koike, N. Fujii, M. Ae, T. Kawamura, and T. Kanahori, A comparison of kinetics in the lower limbs between baseball tee and pitched ball batting. *Hum Mov Sci*, 2018. **61**: p. 126-134.

28. Washington, J. and G. Oliver, Kinematic differences between hitting off a tee versus front toss in collegiate softball players. *International Biomechanics*, 2018. **5**(1): p. 30-35.
29. Marey, E.-J., Animal mechanism: a treatise on terrestrial and aerial locomotion. Vol. 11. 1874: *Henry S. King & Company*.
30. Muybridge, E., Infantile paralysis, child walking on hands and feet. *Animal Locomotion (11 Volumes)*. University of Pennsylvania, Philadelphia, Plate, 1887. **539**.
31. Cuesta-Vargas, A.I., A. Galán-Mercant, and J.M. Williams, The use of inertial sensors system for human motion analysis. *Physical Therapy Reviews*, 2010. **15**(6): p. 462-473.
32. Spörri, J., C. Schiefermüller, and E. Müller, Collecting kinematic data on a ski track with optoelectronic stereophotogrammetry: A methodological study assessing the feasibility of bringing the biomechanics lab to the field. *PloS One*, 2016. **11**(8): p. e0161757.
33. Colyer, S.L., M. Evans, D.P. Cosker, and A.I.T. Salo, A Review of the Evolution of Vision-Based Motion Analysis and the Integration of Advanced Computer Vision Methods Towards Developing a Markerless System. *Sports Medicine - Open*, 2018. **4**(1): p. 24.

34. Yaniv, Z., E. Wilson, D. Lindisch, and K. Cleary, Electromagnetic tracking in the clinical environment. *Medical physics*, 2009. **36**(3): p. 876-892.
35. Schwein, A., B. Kramer, P. Chinnadurai, S. Walker, M. O'Malley, A. Lumsden, and J. Bismuth, Flexible robotics with electromagnetic tracking improves safety and efficiency during in vitro endovascular navigation. *Journal of vascular surgery*, 2017. **65**(2): p. 530-537.
36. Franz, A.M., T. Haidegger, W. Birkfellner, K. Cleary, T.M. Peters, and L. Maier-Hein, Electromagnetic tracking in medicine—a review of technology, validation, and applications. *IEEE transactions on medical imaging*, 2014. **33**(8): p. 1702-1725.
37. Oliver, G.D., H.A. Plummer, and D.W. Keeley, Muscle Activation Patterns of the Upper and Lower Extremity During the Windmill Softball Pitch. *The Journal of Strength & Conditioning Research*, 2011. **25**(6): p. 1653-1658.
38. Oliver, G.D. and H. Plummer, Ground reaction forces, kinematics, and muscle activations during the windmill softball pitch. *Journal of Sports Sciences*, 2011. **29**(10): p. 1071-1077.
39. Plummer, H.A. and G.D. Oliver, The Relationship Between Gluteal Muscle Activation and Throwing Kinematics in Baseball and Softball Catchers. *The Journal of Strength & Conditioning Research*, 2014. **28**(1): p. 87-96.
40. Glossop, N.D., Advantages of optical compared with electromagnetic tracking. *J*

Bone Joint Surg Am, 2009. **91 Suppl 1**: p. 23-8.

41. Ahmad, N., R.A.R. Ghazilla, N.M. Khairi, and V. Kasi, Reviews on various inertial measurement unit (IMU) sensor applications. *International Journal of Signal Processing Systems*, 2013. **1(2)**: p. 256-262.
42. Kan, Y.-C. and C.-K. Chen, A wearable inertial sensor node for body motion analysis. *IEEE Sensors Journal*, 2011. **12(3)**: p. 651-657.
43. Mancini, M., L. Chiari, L. Holmstrom, A. Salarian, and F.B. Horak, Validity and reliability of an IMU-based method to detect APAs prior to gait initiation. *Gait & posture*, 2016. **43**: p. 125-131.
44. Ong, Z.C., Y. Seet, S.Y. Khoo, and S. Noroozi, Development of an economic wireless human motion analysis device for quantitative assessment of human body joint. *Measurement*, 2018. **115**: p. 306-315.
45. Kim, J.-H., S. Sukkarieh, and S. Wishart. Real-time Navigation, Guidance, and Control of a UAV using Low-cost Sensors. in *Field and Service Robotics*. 2003. *Springer*.
46. Kalman, R.E., A new approach to linear filtering and prediction problems. 1960.
47. Sabatini, A.M., Kalman-filter-based orientation determination using inertial/magnetic sensors: Observability analysis and performance evaluation. *Sensors*, 2011. **11(10)**: p. 9182-9206.

48. Julier, S.J. and J.K. Uhlmann. New extension of the Kalman filter to nonlinear systems. in *Signal processing, sensor fusion, and target recognition VI*. 1997. *International Society for Optics and Photonics*.
49. Trinh, X.S., D. Ngoduy, M. Keyvan-Ekbatani, and B. Robertson. A comparative study on filtering methods for online freeway traffic estimation using heterogeneous data. in *2019 IEEE Intelligent Transportation Systems Conference (ITSC)*. 2019. *IEEE*.
50. Mahony, R., T. Hamel, and J.-M. Pflimlin, Nonlinear complementary filters on the special orthogonal group. *IEEE Transactions on automatic control*, 2008. **53**(5): p. 1203-1218.
51. Madgwick, S.O., A.J. Harrison, and R. Vaidyanathan. Estimation of IMU and MARG orientation using a gradient descent algorithm. in *2011 IEEE international conference on rehabilitation robotics*. 2011. *IEEE*.
52. Madgwick, S., An efficient orientation filter for inertial and inertial/magnetic sensor arrays. *Report x-io and University of Bristol (UK)*, 2010. **25**: p. 113-118.
53. Ludwig, S.A. and K.D. Burnham. Comparison of euler estimate using extended Kalman filter, Madgwick and Mahony on quadcopter flight data. in *2018 International Conference on Unmanned Aircraft Systems (ICUAS)*. 2018. *IEEE*.
54. Ludwig, S.A., K.D. Burnham, A.R. Jiménez, and P.A. Touma. Comparison of

- attitude and heading reference systems using foot mounted MIMU sensor data: basic, Madgwick, and Mahony. in *Sensors and Smart Structures Technologies for Civil, Mechanical, and Aerospace Systems 2018*. 2018. *International Society for Optics and Photonics*.
55. Falbriard, M., M. Mohr, and K. Aminian, Hurdle Clearance Detection and Spatiotemporal Analysis in 400 Meters Hurdles Races Using Shoe-Mounted Magnetic and Inertial Sensors. *Sensors*, 2020. **20**(2): p. 354.
56. Caramia, C., D. Torricelli, M. Schmid, A. Muñoz-Gonzalez, J. Gonzalez-Vargas, F. Grandas, and J.L. Pons, IMU-Based Classification of Parkinson's Disease From Gait: A Sensitivity Analysis on Sensor Location and Feature Selection. *IEEE Journal of Biomedical and Health Informatics*, 2018. **22**(6): p. 1765-1774.
57. Wilson, S., H. Eberle, Y. Hayashi, S.O. Madgwick, A. McGregor, X. Jing, and R. Vaidyanathan, Formulation of a new gradient descent MARG orientation algorithm: Case study on robot teleoperation. *Mechanical Systems and Signal Processing*, 2019. **130**: p. 183-200.
58. Koike, S. and S. Tazawa, Quantification of a Ball-Speed Generating Mechanism of Baseball Pitching Using IMUs. *Proceedings*, 2020. **49**(1): p. 57.
59. Mason, B., Ground reaction forces of elite Australian baseball batters. *Biomechanics XB*, 1987. **752**.

60. Lund, R.J. and D. Heefner, Training the Baseball Hitter: What Does Research Say? *Journal of Physical Education, Recreation & Dance*, 2005. **76**(3): p. 27-33.
61. Escamilla, R.F., G.S. Fleisig, C. DeRenne, M.K. Taylor, C.T. Moorman, 3rd, R. Imamura, E. Barakatt, and J.R. Andrews, Effects of bat grip on baseball hitting kinematics. *J Appl Biomech*, 2009. **25**(3): p. 203-9.
62. Fortenbaugh, D., G. Fleisig, A. Onar-Thomas, and S. Asfour, The effect of pitch type on ground reaction forces in the baseball swing. *Sports Biomech*, 2011. **10**(4): p. 270-9.
63. Fleisig, G.S., W.K. Hsu, D. Fortenbaugh, A. Cordover, and J.M. Press, Trunk axial rotation in baseball pitching and batting. *Sports Biomech*, 2013. **12**(4): p. 324-33.
64. Ae, K., S. Koike, and T. Kawamura, Kinetic function of the lower limbs during baseball tee-batting motion at different hitting-point heights. *Sports Biomech*, 2020. **19**(4): p. 452-466.
65. Ae, K., S. Koike, N. Fujii, M. Ae, and T. Kawamura, Kinetic analysis of the lower limbs in baseball tee batting. *Sports Biomech*, 2017. **16**(3): p. 283-296.
66. Laughlin, W.A., G.S. Fleisig, and K.T. Aune..., The effects of baseball bat mass properties on swing mechanics, ground reaction forces, and swing timing. 2016.
67. Cross, R., The sweet spot of a baseball bat. *American Journal of Physics*, 1998. **66**(9): p. 772-779.

68. Cross, R., Impact of a ball with a bat or racket. *American Journal of Physics*, 1999. **67**(8): p. 692-702.
69. Tabuchi, N., T. Matsuo, and K. Hashizume, Bat speed, trajectory, and timing for collegiate baseball batters hitting a stationary ball. 2007.
70. Katsumata, H., K. Himi, T. Ino, K. Ogawa, and T. Matsumoto, Coordination of hitting movement revealed in baseball tee-batting. *Journal of sports sciences*, 2017. **35**(24): p. 2468-2480.
71. Chu, Y., K. Keenan, K. Allison, S. Lephart, and T. Sell, The positive correlation between trunk, leg, and shoulder strength and linear bat velocity at different ball locations during the baseball swing in adult baseball hitters. *Isokinetics and exercise science*, 2015. **23**(4): p. 237-244.
72. Tago, T., K. Kaneko, D. Tsuchioka, N. Ishii, and T. Wada, Influence of the ball speed on the displacement of the center of gravity during baseball batting motion. *ISBS Proceedings Archive*, 2017. **35**(1): p. 57.
73. Ae, K. and S. Koike. Kinetic analysis of each hand in baseball batting motion at different hitting point heights. in *ISBS-Conference Proceedings Archive*. 2011.
74. Winter, D.A., Biomechanics and motor control of human movement. 2009: *John Wiley & Sons*.
75. Gray, R., Changes in Movement Coordination Associated With Skill Acquisition in

- Baseball Batting: Freezing/Freeing Degrees of Freedom and Functional Variability. *Frontiers in Psychology*, 2020. **11**: p. 1295.
76. Nakata, H., A. Miura, M. Yoshie, T. Higuchi, and K. Kudo, Differences in trunk rotation during baseball batting between skilled players and unskilled novices. *The Journal of Physical Fitness and Sports Medicine*, 2014. **3**(4): p. 457-466.
77. Szymanski, D.J. and C. DeRenne, The effects of small muscle training on baseball hitting performance: A brief review. *Strength & Conditioning Journal*, 2010. **32**(6): p. 99-108.
78. Szymanski, D.J., J.S. McIntyre, J.M. Szymanski, T.J. Bradford, R.L. Schade, N.H. Madsen, and D.D. Pascoe, Effect of torso rotational strength on angular hip, angular shoulder, and linear bat velocities of high school baseball players. *The Journal of Strength & Conditioning Research*, 2007. **21**(4): p. 1117-1125.
79. Pasciuto, I., G. Ligorio, E. Bergamini, G. Vannozzi, A.M. Sabatini, and A. Capozzo, How angular velocity features and different gyroscope noise types interact and determine orientation estimation accuracy. *Sensors*, 2015. **15**(9): p. 23983-24001.
80. Phillips, W.F., C.E. Hailey, G. Gebert, and E. Afb. A Review of Attitude Kinematics for Aircraft Flight Simulation. 2000.
81. Diebel, J., Representing attitude: Euler angles, unit quaternions, and rotation vectors. *Matrix*, 2006. **58**(15-16): p. 1-35.

82. Kuipers, J.B., Quaternions and rotation sequences: a primer with applications to orbits, aerospace, and virtual reality. 1999: *Princeton university press*.
83. Grood, E.S. and W.J. Suntay, A joint coordinate system for the clinical description of three-dimensional motions: application to the knee. *Journal of biomechanical engineering*, 1983. **105**(2): p. 136-144.
84. Wu, G., S. Siegler, P. Allard, C. Kirtley, A. Leardini, D. Rosenbaum, M. Whittle, D. D D'Lima, L. Cristofolini, and H. Witte, ISB recommendation on definitions of joint coordinate system of various joints for the reporting of human joint motion—part I: ankle, hip, and spine. *Journal of biomechanics*, 2002. **35**(4): p. 543-548.
85. Cole, G., B. Nigg, J. Ronsky, and M. Yeadon, Application of the joint coordinate system to three-dimensional joint attitude and movement representation: a standardization proposal. *Journal of biomechanical engineering*, 1993. **115**(4A): p. 344-349.
86. Graf, B., Quaternions and dynamics. *arXiv preprint arXiv:0811.2889*, 2008.
87. Bergmann, J.H.M., R.E. Mayagoitia, and I.C.H. Smith, A portable system for collecting anatomical joint angles during stair ascent: a comparison with an optical tracking device. *Dynamic Medicine*, 2009. **8**(1): p. 3.
88. Zhou, H., T. Stone, H. Hu, and N. Harris, Use of multiple wearable inertial sensors in upper limb motion tracking. *Medical engineering & physics*, 2008. **30**(1): p. 123-

- 133.
89. Koo, T.K. and M.Y. Li, A guideline of selecting and reporting intraclass correlation coefficients for reliability research. *Journal of chiropractic medicine*, 2016. **15**(2): p. 155-163.
90. Altman, D.G. and J.M. Bland, Measurement in medicine: the analysis of method comparison studies. *Journal of the Royal Statistical Society: Series D (The Statistician)*, 1983. **32**(3): p. 307-317.
91. Slade, P., A. Habib, J.L. Hicks, and S.L. Delp, An open-source and wearable system for measuring 3D human motion in real-time. *IEEE Transactions on Biomedical Engineering*, 2021: p. 1-1.
92. Chambers, R., T.J. Gabbett, M.H. Cole, and A. Beard, The Use of Wearable Microsensors to Quantify Sport-Specific Movements. *Sports Medicine*, 2015. **45**(7): p. 1065-1081.
93. Shepherd, J.B., D.A. James, H.G. Espinosa, D.V. Thiel, and D.D. Rowlands, A literature review informing an operational guideline for inertial sensor propulsion measurement in wheelchair Court sports. *Sports*, 2018. **6**(2): p. 34.
94. Dahl, K.D., K.M. Dunford, S.A. Wilson, T.L. Turnbull, and S. Tashman, Wearable sensor validation of sports-related movements for the lower extremity and trunk. *Medical Engineering & Physics*, 2020. **84**: p. 144-150.

95. Cust, E.E., A.J. Sweeting, K. Ball, and S. Robertson, Classification of Australian football kick types in-situation via ankle-mounted inertial measurement units. *Journal of Sports Sciences*, 2021: p. 1-9.
96. McGrath, J., J. Neville, T. Stewart, and J. Cronin, Upper body activity classification using an inertial measurement unit in court and field-based sports: A systematic review. *Proceedings of the Institution of Mechanical Engineers, Part P: Journal of Sports Engineering and Technology*, 2020: p. 1754337120959754.
97. Koike, S. and S. Tazawa. Quantification of a Ball-Speed Generating Mechanism of Baseball Pitching Using IMUs. in *Multidisciplinary Digital Publishing Institute Proceedings*. 2020.
98. Lapinski, M., E. Berkson, T. Gill, M. Reinold, and J.A. Paradiso. A distributed wearable, wireless sensor system for evaluating professional baseball pitchers and batters. in *2009 International Symposium on Wearable Computers*. 2009. *IEEE*.
99. Lizzio, V.A., E.W. Guo, and E.C. Makhni, Monitoring the Throwing Motion: Current State of Wearables and Analytics, in *Elbow Ulnar Collateral Ligament Injury*. 2021, *Springer*. p. 27-35.
100. Van Zandt, L., The dynamical theory of the baseball bat. *American Journal of Physics*, 1992. **60**(2): p. 172-181.
101. King, K., J. Hough, R. McGinnis, and N.C. Perkins, A new technology for resolving

- the dynamics of a swinging bat. *Sports Engineering*, 2012. **15**(1): p. 41-52.
102. Greenwald, R.M., L.H. Penna, and J.J. Crisco, Differences in batted ball speed with wood and aluminum baseball bats: a batting cage study. *Journal of applied Biomechanics*, 2001. **17**(3): p. 241-252.
103. Nathan, A.M., Dynamics of the baseball–bat collision. 2000.
104. Horiuchi, G. and S. Sakurai, Kinetic Analyses on Increase of Bat Head Speed in Baseball Batting. *International Journal of Sport and Health Science*, 2016. **14**: p. 94-101.
105. Nicholls, R.L., K. Miller, and B.C. Elliott, Numerical analysis of maximal bat performance in baseball. *Journal of biomechanics*, 2006. **39**(6): p. 1001-1009.
106. Cochran, W.G., Errors of measurement in statistics. *Technometrics*, 1968. **10**(4): p. 637-666.
107. Lesk, A.M., On the calculation of Euler angles from a rotation matrix. *International Journal of Mathematical Education in Science and Technology*, 1986. **17**(3): p. 335-337.
108. De Vries, W., H. Veeger, C. Baten, and F. Van Der Helm, Magnetic distortion in motion labs, implications for validating inertial magnetic sensors. *Gait & posture*, 2009. **29**(4): p. 535-541.
109. Li, Q. and J.G. Griffiths. Least squares ellipsoid specific fitting. in *Geometric*

Modeling and Processing, 2004. Proceedings. 2004.

110. NCEI. *Magnetic field caculators*. [cited 2021 November 11]; Available from:

<https://www.ngdc.noaa.gov/geomag/calculators/magcalc.shtml#igrfwmm>.